Magneto-Optical Trapping of Lithium-6 Atoms

Wang Yibo

(Bachelor of Science, University of Science and Technology of China)

A THESIS SUBMITTED

FOR THE DEGREE OF MASTER OF

SCIENCE

DEPARTMENT OF PHYSICS

NATIONAL UNIVERSITY OF SINGAPORE

June 2012

Acknowledgements

I would like to thank my supervisor Asst Prof. Wenhui Li. Thank her for providing me the opportunity to study in the Quantum Matter Group in Centre for Quantum Technologies, NUS. It is my honour to work in this wonderful group. Thanks very much for her careful guidance and warm encouragements. I also like to express my great gratitude to Assoc Prof. Kai Dieckmann. I always benefit from his smart ideas and deep physical insights.

I also like to thank our Postdoc. Jimmy Sebastian. He is not only a good researcher with rich experience but also a elder brother who helps me with great patience from the very beginning of this project. Thanks also to everyone in our big group, Lim Chin Chean, Thi Ha Kyaw, Christian Gross, Thong May Han, Ke Li, Tarun Johri, Kanhaiya Pandey, Sambit Bikas Pal, Johannes Gambari and Lam Mun Choong Mark.

Many thanks to Bob Chia Zhi Neng, Teo Kok Seng, Gan Eng Swee, Mohammad Imran, Yau Yong Sean and Lian Chorng Wang. Without their excellent supporting works this project cannot be proceeded so smoothly.

I have to say thanks to many good friends. They always give me warm hands when i am trapped in troubles. Their friendship is the invaluable treasure in my life.

Finally, I want to thank my parents. I miss them so much!

Contents

Summary

An apparatus has been developed which allows for the creation of cold sample of ^6Li atoms. As the first stage of the whole experiment, the apparatus will be a stable and versatile platform for the further experiment, UV cooling, evaporation cooling in optical dipole trap and 2D optical lattices.

This thesis will primarily detail the construction of vacuum system and laser system for the red(671nm) magneto-optical trap(MOT) of ^6Li atoms, experimental operation as well as current results. At last, UV(323nm) cooling strategy is briefly discussed. The UV Doppler free absorption signal and error signal will allow us to pursue the UV MOT in the near future.

List of Tables

List of Figures

1. Introduction

1.1 From BEC to DFG

Combining laser cooling and evaporate cooling technique, scientists finally achieved Bose-Einstein Condensate(BEC) in dilute gases in 1995[1–3], 70 years after Satyendra Nath Bose and Albert Einstein first predicted this state of matter[4, 5]. Four years later, sympathetic cooling technique overcame Pauli exclusion principle[6] and led to the creation of quantum Degeneracy Fermion Gases(DFG)[7]. Ultracold quantum gases allow us to study the similar quantum many body physics which is much more difficult to probe in other systems, such as condensed matter physics and high energy physics. DFG is particularly interesting since fermions comprise the fundamental building blocks of matter: protons, neutrons, and electrons. They can be the direct quantum simulator of High temperature superconductivity and Superfluidity of Helium-3 in condensed matter physics.

Lithium-6(^6Li) and potassium-40(^{40}K) are the most widely investigated fermionic species in the laboratories all over the world, they are two stable fermionic isotopes among the alkali metals. ^6Li is especially suited for exploring quantum many body physics in the strongly interaction regime. Since for a spin mixture the interactions between two spin components can be tuned across a broad Feshbach resonance[8] at accessible magnetic fields. Because of the unusually large and negative triplet scattering length[9], ultracold ^{6}Li is considered a possible candidate for investigations of superfluid transition[10]. Also it represents the most hydrogen-like element. Many properties of lithium can therefore be calculated from first principles which allows for precision measurements of fundamental quantities. First DFG of ^6Li were achieved in three different groups in 2001. John Thomas' group at Duke University created DFG by direct evaporation the two lowest hyperfine states of ^6Li confined in optical trap[11]. Randall Hulet's group at Rice University and Christophe Salomon's group at ENS formed DFG by evaporating the two-species mixture of ^6Li and ^7Li in magnetic trap[12, 13].

Fermion lattice project in Centre for Quantum Technology(CQT), National University of Singapore(NUS) plans to produce degenerate lithium gas with an all-optical method. Ultracold ^6Li atoms will be loaded into 2D optical lattices. Optical lattices[14] offers a fully controlled way to investigate many interesting but not well-understood phenomena in condensed matter physics. Such as fractional quantum hall effect under rotation[15], transport properties of massless Dirac fermions[16]. Achieving red(671nm) MOT of ^6Li is just the starting point of this long journey. Further experimental development will grow from this base. Therefore, creating and optimizing the red MOT is important for the future experiment.

1.2 Outline

This thesis presents detailed description of building up the experiment. It contains three major sections: vacuum system, laser system, and UV spectroscopy. The thesis is organized as below:

- Chapter 2 gives an introduction of theoretical concepts which are essential for the experiments described in this thesis.
- Chapter 3 describes the vacuum system for the experiment.
- Chapter 4 details the $671nm$ laser system for the red MOT.
- Chapter 5 represents the red MOT of ^6Li.
- Chapter 6 reports the UV spectroscopy of ^6Li which employs $|2^2S_{1/2}\rangle \rightarrow |3^2P_{3/2}\rangle$ transition.

2. Theory

This chapter presents related theoretical background. Basic concepts of laser cooling and trapping are discussed. Laser cooling and trapping theory will guide the design and procedure of experiment.

2.1 Kinetic Theory of Gases

In thermodynamics, Maxwell-Boltzmann(MB) distribution is the velocity distribution when system reaches thermal equilibrium with its surroundings. In 3D case, the MB distribution is given by

$$f(v) = \frac{4}{\sqrt{\pi}} \frac{v^2}{v_{mp}^3} exp\left(-\frac{v^2}{v_{mp}^2}\right), \tag{2.1}$$

where v is the velocity of atoms; $v_{mp} = \sqrt{\frac{2K_BT}{M}}$ is the most probable velocity for the distribution; M is the mass of the atom; T is the temperature; K_B is Boltzmann constant.

Lithium is in solid form at room temperature. In order to cooling and trapping lithium atoms, the metal chunk is heated in an oven at 330℃ to create lithium vapor. The most probable velocity is about $1290 m/s$ at this temperature.

2.2 The Scattering Force

The principle of laser cooling was first suggested by T.W. Hänsch and A.L. Schawlow[17] for neutral atoms, and by D. Wineland and H. Dehmelt[18] for trapped ions.

Atomic beam can be slowed by single laser beam. Each absorbed photon gives the atom a momentum kick in the direction opposite to its motion, then spontaneously-emitted photon goes in random direction, so on average the scattering of many photons gives an force that slows the atom down. The scattering force equals:

$$F_{scatt} = \hbar k \cdot R_{scatt} \tag{2.2}$$

The scatter rate

$$R_{scatt} = \frac{\Gamma}{2} \frac{I/I_{sat}}{1 + I/I_{sat} + 4\left(\delta + \omega_D\right)^2/\Gamma^2} \tag{2.3}$$

where k is the wave vector, Γ is the linewidth of the laser, $\delta = \omega - \omega_0$ is laser detuning, $\omega_D = -\vec{k} \cdot \vec{v}$ is the Doppler shift seen by the moving atoms, I is the intensity of laser, $I_{sat} = \pi hc/\left(3\lambda^3\tau\right)$ is the saturation intensity. When $I \to \infty$, the maximum scattering force $F_{scatt} = F_{max} = \hbar k\Gamma/2$ and the maximum acceleration $a_{max} = \dfrac{F_{max}}{M} = \dfrac{\hbar k\Gamma}{2M}$.

In Lab condition, however, usually $F_{scatt} = F_{Lab} = F_{max}/2$. For ^6Li, the relative values are listed in Table(2.1)

Mass	M	$9.988 \times 10^{-27} kg$
Wavelength of D2 line	λ	$670.978 \times 10^{-9} m$
Lifetime of D2 line	τ	$27.102 \times 10^{-9} s$
Saturate intensity	I_{sat}	$25.408 W/m^2$
Maximum scattering force	F_{max}	$1.822 \times 10^{-20} N$
Maximum acceleration	a_{max}	$1.824 \times 10^{6} m/s^2$
Realized acceleration	a_{Lab}	$9.125 \times 10^{5} m/s^2$

Table 2.1: Optical properties of ^6Li D2 line.

For constant deceleration, if we choose initial velocity $v_0 = 1290 m/s$(the most probable velocity of lithium at 330℃), $a = a_{Lab}$, the stopping distance is about $0.9m$. It can be said that laser beam is a very powerful tool for slowing atoms.

2.3 The Spin-Flip Zeeman Slower

The change of Doppler shift caused by deceleration, however, will bring atoms out of resonance with laser beam. The whole deceleration process is stop then. In order to maintain deceleration and slow atoms from speed of more than one thousand meter per second down to tens meter per second(the range of MOT capture velocity), it is necessary to compensate the change of Doppler shift. One method is to create a special magnetic field profile along the deceleration axis that Zeeman shift caused by the magnetic field exactly compensate the change of Dopper shift in each point of the axis. The first successful experiment of slowing atomic beam using so called Zeeman slower was demonstrated by William Phillips[19].

The Zeeman slower is usually a tube winding with tapered solenoid coil which is

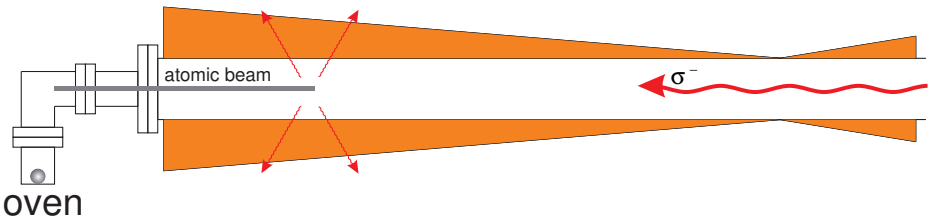

Figure 2.1: The Spin-Flip Zeeman slower. The Zeeman shift caused by special designed magnetic field compensates the change of Dopper shift, therefore maintains the whole deceleration.

shown in Fig(2.1). The frequency shift caused by the Zeeman effect obeys the condition:

$$\omega_0 + \frac{\mu_B B(z)}{\hbar} = \omega + kv \tag{2.4}$$

The required magnetic filed profile is:

$$B(z) = B_0\sqrt{1 - \frac{z}{L_0}} + B_{bias} \tag{2.5}$$

where $B_0 = \dfrac{hv_0}{\lambda\mu_B}$, if $B_{bias} = \dfrac{\hbar}{\mu_B}(\omega - \omega_0)$, the atoms completely stop at the end of the slower. For further cooling and trapping atoms, it is useful to leave atoms with a small velocity so that they can reach the MOT area.

A spin-flip Zeeman slower is designed for our experiment(Fig(2.1)). In such configuration, the direction of the magnetic field switches, however, the spin direction of the atoms maintain the same along the Zeeman slower. The magnetic field profile of spin-flip Zeeman slower is realized by two successive main coils both producing fields parallel to the atomic beam but with opposite directions. An additional compensation coil on the opposing side of the MOT chamber compensates the stray field of the Zeeman slower at the center position of the MOT chamber.

A spin-flip Zeeman slower has several advantages compare to other designs:

First, by choosing a magnetic field with opposite directions at the two ends of the Zeeman slower, the absolute field strength necessary is reduced, therefore less current is needed and the power dissipation is decreased.

Second, the absolute value of the magnetic field increases at the exit of the Zeeman slower. A Zeeman slower with an increasing magnetic field is more efficient and much less sensitive to variations in the laser intensity and detuning than one with a decreasing magnetic field[20].

Third, this configuration produces less field in MOT chamber, since the contribution from the two coils tend to cancel each other.

The slower tube is a $0.714m$ long hollow steel tube with outer and inner diameters of $54mm$ and $45.1mm$, respectively. Cooling water limits the temperature below 60℃ avoid Zeeman coil melt at higher temperature. The wire has comparatively large rectangular cross section(Isodraht, $4mm \times 1mm$) and is electrically insulated by heat resistant varnish. The winding procedure accomplished with the help of lathe. Finally the coil is glued(Loctite, Hysol $9492A\&B$) to improve heat conductance and mechanical stabilization.

The slower has an effective length of about $0.6m$. The capture velocity is estimated at $1045m/s$ where as the most probable velocity is around $1290m/s$. About 27.4% of the total atoms will be slowed down by the slower. The velocity at the end of the slower is setted to be $80m/s$. The realized deceleration rate of the slower is $9.1 \times 10^5 m/s^2$. The bias field is setted to be $-390G$, then the detuning of slower laser beam is $-448MHz$ from $|2^2S_{1/2}, F = 1/2\rangle \rightarrow |2^2P_{3/2}\rangle$ and $|2^2S_{1/2}, F = 3/2\rangle \rightarrow |2^2P_{3/2}\rangle$ transitions. Fig(2.2) shows the numerical simulation results:

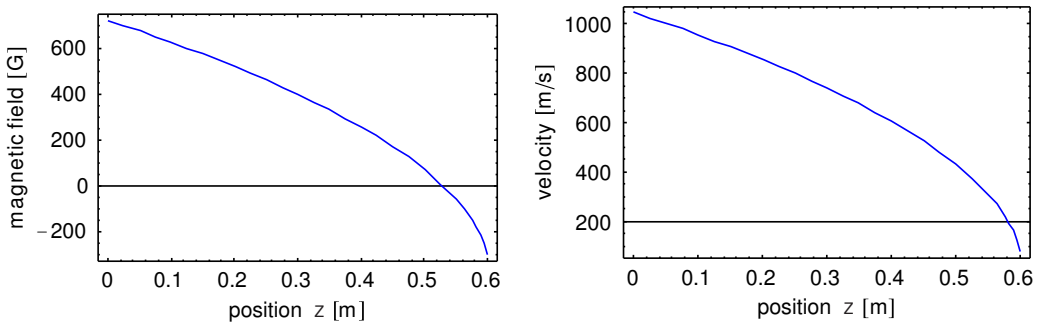

Figure 2.2: Magnetic field and deceleration of designed Zeeman slower. Z direction indicts the Zeeman slower axis. The effective length of Zeeman slower is $0.6m$. The operation current is $10A$.

2.4 Optical Molasses

Atoms in a gas can move in all directions. The configuration of 3D optical molasses[21] shown in Fig(2.3) will reduce the temperature of atom sample in all three directions. The frictional force exerted on atoms in optical molasses just like that on a particle in a viscous fluid.

To understand the principle of optical molasses, let us first considering a moving two-level atom in 1D optical molasses configuration. Assume laser frequency below the atomic resonance frequency, the Doppler effect brings the frequency of the laser beam propagating in the direction opposite to the atom's velocity closer to resonance. This leads to an imbalance in the scattering forces which slows atom down:

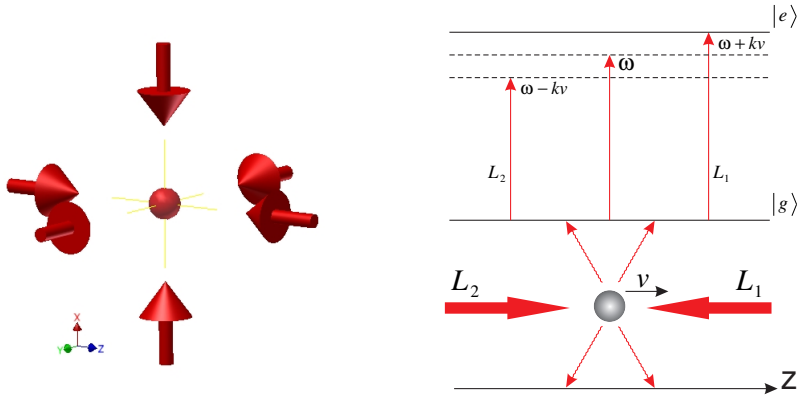

(a) 3D optical molasses configuration. **(b)** 1D optical molasses.

Figure 2.3: Optical molasses. (a)The configuration of three orthogonal pairs of counter-propagating laser beams. (b)For a moving atom, the Doppler effect leads more scattering in the opposite direction of the velocity.

$$\begin{aligned} F_{molasses} &= F_{scatt}\left(\omega-\omega_0-kv\right)-F_{scatt}\left(\omega-\omega_0+kv\right) \\ &\simeq -4\hbar k^2\frac{I}{I_{sat}}\frac{-2\delta/\Gamma}{\left[1+I/I_{sat}+(2\delta/\Gamma)^2\right]^2}v \qquad (2.6) \\ &\equiv -\alpha v \qquad (2.7) \end{aligned}$$

Low velocity $kv \ll \Gamma$ have been assumed. α is the damping coefficient. Damping requires a positive value of α and hence $\delta = \omega - \omega_0 < 0$ (red detuning). The damping force in 1D optical molasses(Fig(2.4)) has a negative gradient $\partial F/\partial v < 0$ at $v = 0$. It is convenient to define a capture velocity of optical molasses $v_{c_{OM}} \equiv \Gamma/k$. For ^6Li, $v_{c_{OM}} = 3.94m/s$.

Similar result in 3D case, the kinetic energy $E = \frac{1}{2}M\left(v_x^2+v_y^2+v_z^2\right)$ of an atom in the intersection region of three orthogonal pairs of laser beams decreases as:

$$\frac{dE}{dt} = -\frac{2\alpha}{M}E \qquad (2.8)$$

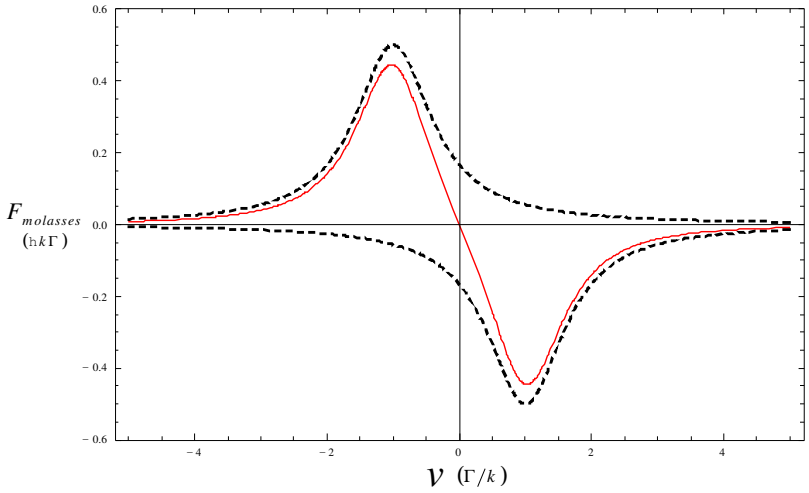

Figure 2.4: The scattering force as a function of the velocity in 1D optical molasses. $\delta = -\Gamma$, the force is negative for $v > 0$ and positive for $v < 0$. (k is the wave vector.) The force confines atoms in original point.

It will give us a nonphysical prediction that all atoms will be decelerated to $v = 0$ and energy of the sample tends to zero($T = 0$) in the end.

On above, we just consider the average condition. However, each spontaneous emission photon also gives atom a recoil kick in random directions. These recoil kicks lead to a random walk of the velocity. This random walk causes diffusive heating. The equilibrium temperature is determined by the balance between this diffusive heating and the Doppler cooling:

$$k_B T = \frac{\hbar\Gamma}{4} \frac{1 + (2\delta/\Gamma)^2}{-2\delta/\Gamma} \tag{2.9}$$

This function has a minimum at $\delta = -\Gamma/2$ of

$$k_B T_D = \frac{\hbar\Gamma}{2} \tag{2.10}$$

The Doppler temperature T_D set the cooling limit of optical molasses. For ^6Li, $T_D = 141\mu K$.

Soon much lower temperature measured in experiment[22]. This strong violation of Doppler cooling limit forced scientists to recheck theory model. Since real atoms are not two-level toy models, the Doppler temperature derived from two-level system is inadequate. To understand the mechanics of sub-Doppler cooling, multi-level structure of atoms must be considered. The sub-Doppler cooling theory which considers multi-level atomic structure and optical pumping was quickly proposed in two

groups independently[23, 24]. The limit of sub-Doppler cooling is the recoil temperature $T_r = \frac{Mv_r^2}{k_B}$. Recoil velocity is $v_r = 9.88cm/s$, $T_r = 7.06\mu K$ for ^6Li.

2.5 Magneto-Optical Trap

Although atoms confined in optical molasses take a considerable time(several seconds for beams of $1cm$ radius) to diffuse out, optical molasses is not a trap for neutral atoms because there is no restoring force on atoms when they have been displaced from the center.

Optical molasses configuration can be turned into a trap by adding a pair of Helmholtz coils and choosing correct polarization of the laser beams, as illustrated in Fig(2.5). The two coils with currents in opposite directions produce a quadrupole magnetic field. The quadrupole magnetic field causes an imbalance in the scattering forces of the laser beams which strongly confines the atoms. The first magneto-optical trapping was demonstrated in 1987[25].

The principle of the MOT can be simply understood in 1D for a $J = 0$ to $J = 1$ transition(Fig(2.5)).

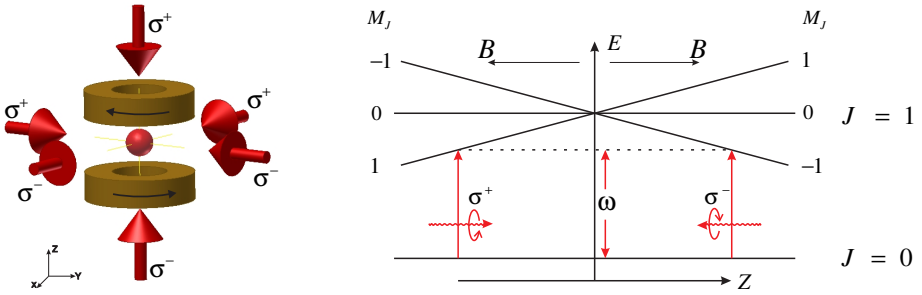

(a) MOT configuration. **(b)** The mechanism of MOT illustrated in 1D.

Figure 2.5: MOT configuration. (a)A pair of Helmholtz coils with currents in opposite directions. Three pair of laser beams have required polarization. (b)The magnetic fields cancel out in geometrical center of the coils. There is a uniform field gradient near the geometrical center. So the Zeeman effect causes the energy of the sub-levels(with $M_J = 0, \pm 1$) of the $J = 1$ level to vary linearly with the atom's position near the center. The red-detuning counter-propagating laser beams have circular polarization drive atoms to different excited states.

Considering an atom displaced from the center of the trap along z-axis with $z > 0$, so the $\Delta M = -1$ transition becomes more closer to resonance with the laser frequency which increases the rate of absorption. The selection rules allow atom to absorb photons from the σ^- beam. This gives a scattering force that push the atom back towards the

trap center($z = 0$). A similar process occurs for a displacement in the opposite direction ($z < 0$), in this case the σ^+ beam pushes the atom back towards the trap center.

To describe the MOT mathematically,

$$F_{MOT} = F^{\sigma^+}_{scatt}(\omega - kv - (\omega_0 + \beta z)) - F^{\sigma^-}_{scatt}(\omega + kv - (\omega_0 - \beta z)) \quad (2.11)$$

$$\simeq -\alpha v - \frac{\alpha\beta}{k} z \quad (2.12)$$

Where $\beta z = \frac{g\mu_B}{\hbar}\frac{dB}{dz}z$ is the Zeeman shift at displacement z. The spring constant of restoring force is $\alpha\beta/k$. The position-dependent force pushes the atoms back to the trap center when atoms enter the region of intersection of the laser beams. Since the laser light is red detuning($\delta < 0$), $\alpha > 0$, cooling and compression of the atoms is simultaneously obtained in a MOT. The force leads to damped harmonic motion of atoms, where the damping rate is given by $\Gamma_{MOT} = \alpha/M$ and oscillation frequency $\omega_{MOT} = \sqrt{\alpha\beta/kM}$. Typically, the oscillation frequency is a few KHz, whereas the damping rate is a few hundred KHz. Thus the motion is overdamped.

The magnetic field gradients in a MOT are much smaller than those used in magnetic traps. So the Helmholtz coils can easily be achieved with simple air-cooled coils. A typical magnetic field gradient is a few $10G/cm$. When laser beams are switched off the magnetic force produced by the Helmholtz coils is not sufficient to support atoms against gravity. In our experiment, two water cooled MOT coils are installed in upper and lower side of the MOT chamber. The magnetic gradients in axis direction is $30G/cm$, and $12G/cm$ in transverse direction for the red MOT(Fig(2.6)).

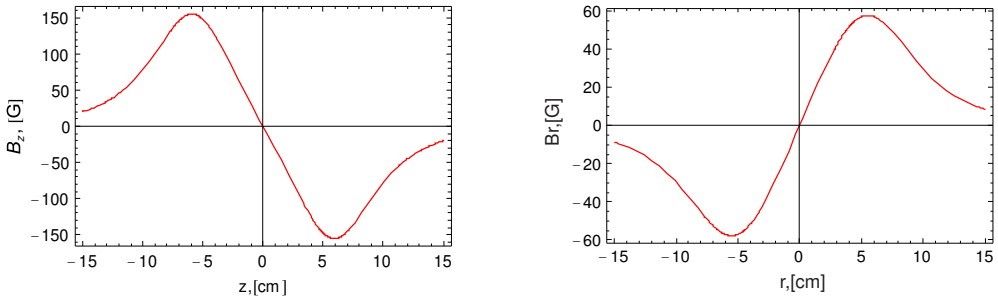

Figure 2.6: Magnetic field of MOT. The current of MOT coils is 15A.

The capture velocity $v_{c_{MOT}}$ of the MOT is given by the incoming velocity for which atoms are completely stopped when they reach the opposite edge of the MOT region. A roughly estimation is given by $v_{c_{MOT}} = \sqrt{2a_{max}D}$, D is the diameter of laser beam.

For $1cm$ laser beam, the capture velocity is about $130m/s$.

At equilibrium each atom absorbs and emits the same amount of light. Therefore a large cloud of cold atoms in the MOT scatters a significant mount of light so that the atoms can be seen by the naked eyes as a bright glowing ball. Measuring the fluorescence of the MOT provides the information of lifetime, atom number and size of the MOT. In good vacuum conditions, the lifetime of MOT is on the order of 1s. The temperature of the MOT can be extracted from the time of flight(TOF) measurement[26]. The steady-state temperature of atoms in a MOT is expected to be comparable to the temperature for optical molasses.

This combination of strong damping and trapping makes the magneto-optical trap easy to load and it is very widely used in laser cooling experiments. Typically, an MOT loaded from a slow atomic beam contains up to 10^{10} atoms.

3. Vacuum System

The experimental platform for the generation of ^6Li MOT contains two major parts: vacuum system and laser system, which locate on different optical tables. My master work is mainly to build up this platform. Therefore, the design and construction of this apparatus is the major part of the thesis.

This chapter describes the vacuum system, the laser system will be discussed in next chapter. In cold atom experiments, atoms are cooled and trapped in an vacuum chamber. The purpose of the vacuum chamber is to isolate the atoms under study from the atmosphere environment. Generally, experimentalists attempt to achieve the highest vacuum as they can. In our setup, the vacuum pressure of the MOT chamber has been achieved and maintained at around $7.5 \times 10^{-11} mbar$. It is good enough for the MOT experiment.

3.1 Setup

The design of the vacuum system is basically a copy of the apparatus which built in Munich group[27]. The vacuum system is shown in Fig(3.1). It consists of three main sections: oven chamber, Zeeman slower and MOT chamber. The oven chamber allows loading lithium and gives a collimated atomic beam. The MOT chamber is a spherical octagon bought from KIMBALL PHYSICS(MCF800-SO2000800). Cold atoms are cooled and trapped in the center of this chamber. Zeeman slower connects the oven chamber and the MOT chamber. It slows atoms and loads them into MOT. In order to avoid stray magnetic field, all the vacuum components are made of steel with a low magnetic permeability(316/A4 steel).

The oven chamber starts with a lithium oven which is connected to a CF63 five-cross through a nozzle($6mm$ inner diameter, $165mm$ length) to collimate the atomic flux. The atomic beam can be blocked by a mechanical shutter driven by an all metal rotation feed-through(VTS Schwarz, TMR40). Two CF63 viewports supply optical access to the oven chamber for spectroscopic analysis of the lithium atom beam as well as for general

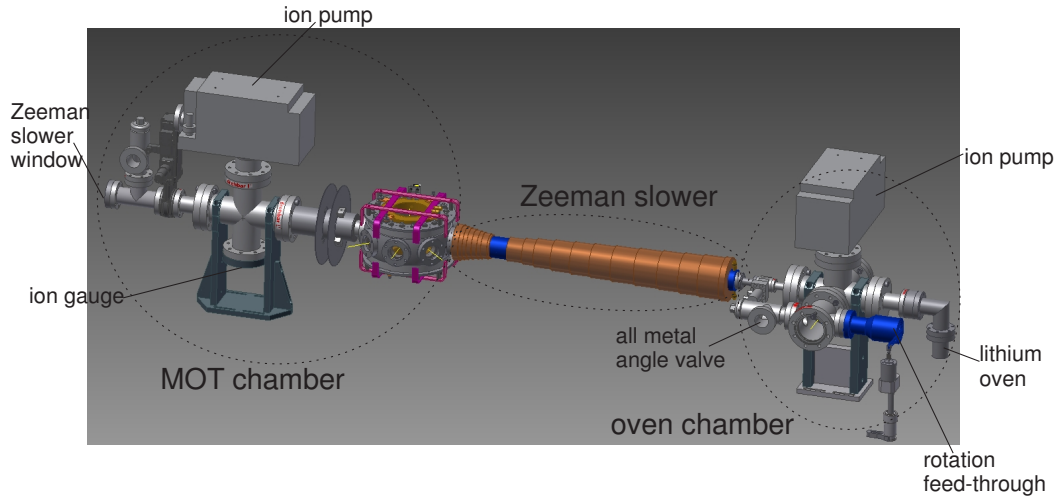

Figure 3.1: Vacuum system. The graph shows a 3D-CAD drawing of the vacuum chambers.

visual inspection. The oven chamber is pumped by an ion pump(Varian, VacIon Plus 75 StarCell)and sealed by an all metal angle valve(Vacom GMV-40R) which permits us to connect a roughing pump for initial pumping. A pneumatically actuated valve(HVA 11223-0064) separates oven chamber from Zeeman slower and the MOT chamber, allows reloading lithium without breaking the whole vacuum system. On both sides of the pneumatically actuated valve, two tubes($6mm$ inner diameter, $133mm$ length and $6mm$ inner diameter, $103mm$ length) make up of the differential pumping stage.

The oven chamber and the MOT chamber are connected by a $0.783m$ long homemade steel tube(Zeeman tube), around which the Zeeman slower coil is installed. The inner diameter of the Zeeman tube increases from $16mm$(this end is installed one differential pumping tube) to $38mm$ along the lithium beam flux direction. So the Zeeman slower can be efficiently pumped from the larger end connected to the MOT octagon. By carefully align the nozzle and two differential pumping tubes, the atomic beam can go through the geometric center of the MOT octagon.

The MOT chamber is pumped through a CF63 four-cross by a ion pump(Varian, VacIon Plus75 StarCell). An ion gauge(Varian, UHV-24P) is installed to measure the pressure of the MOT chamber. The last port of the four-cross is connected a tee piece, a viewport is flanched for the Zeeman slowing laser beam. This viewport(Zeeman slower window) is heated at 90℃ to prevent permanent coating with incident lithium atoms. A same kind of all metal angle valve is also connected for initial pumping. After desired vacuum is achieved, MOT coils and air compensation coils will be installed surrounding

the spherical octagon chamber. The MOT compensation coil also needed to fixed in other side of the MOT chamber to complete the spin-flip Zeeman slower configuration.

3.2 Vacuum Components Cleaning

In order to achieve ultra-high vacuum(UHV)[28], all the components should be properly cleaned. Components should be carefully inspected after unpacking, especially the knife-edges. If they are notched, scratched, bent, or blunted then they cannot be used any more. For other obvious contaminates, e.g. chunks of dirt, they can be removed by lens tissue paper and solvent(Acetone).

It is the time to clean these components after inspection. For most structural components of a UHV system, including flanges, elbows, tees, crosses, chambers, and anything else made of stainless steel, we basically follow the cleaning procedure as below:

① Ultrasound the components for 30 minutes in distilled water at 70℃.

② Ultrasound the components for 30 minutes in detergent at 70℃.

③ Ultrasound the components for 30 minutes in distilled water at 70℃.

④ Ultrasound the components for 30 minutes in distilled water at 70℃ again.

⑤ Ultrasound the components for 30 minutes in acetone at 30℃.

⑥ Packed with aluminium foil

For more delicate components(viewport, ion gauge and feedthrough), check the menu and contact the technicians first.

3.3 Vacuum System Assembling and Loading Lithium

Before starting assembling the system, make sure all the vacuum components have been properly cleaned. Preparing plenty of gaskets, nuts, washers, bolts, powder free gloves, aluminum foil, tissue paper, solvents and anti-seize compound(Loctite 51609). It is suggested that start pumping the whole system as soon as possible after assembling instead of exposing it in atmosphere for long time. Since the small particles and dirts in the air will pollute vacuum components.

Carefully placing the gasket between the knife edges. Only touch the outer edge

of a gasket with clean gloves. Anti-seize compound is suggested to put on the threads of bolts. Tighten the bolts with hand before tightening any of them with a wrench. Residual gas analyzer(SRS RGA200) is installed near the turbo-molecular pump for leak test.

Lithium should be loaded in oven before pumping. Since lithium is quickly oxidized when it contacts with the air, we have to find a way of cutting and loading it into the oven without any air contact.

Lithium chunks with 95% abundance of ^6Li(Sigma-Aldrich 340421-10G) are cut into small pieces with clean razor blade in an air bag(Sigma-Aldrich AtmosBag) filled with ultra-high purity(UHP) Argon. The lithium chunks sealed in kerosene in a glass bottle. Using tweezers to take the lithium chunks out, the kerosene should be carefully cleaned with lens tissue paper and acetone since kerosene is very bad for making UHV. Then removing the black surface with clean razor blade until the surface of lithium become silver-white. Make sure that only pure lithium chunks will be put into oven. The whole vacuum system should be flushed with UHP Argon instead of exposing in the atmosphere. Monitor the pressure of argon from pressure meter on the gas cylinder, it can never be larger than $1bar$. Otherwise, the viewports of vacuum system will be easily broken. Usually $0.5bar$ is chosen for safety. Finally, transfer the shining lithium pieces quickly into oven cap and closing the whole system.

3.4 Pumping and Baking the System

An oil-free roughing pumping system consisting of a turbo-molecular pump(Pfeiffer TMU 071P) and a diaphragm pump(Pfeiffer MVP 035-2) is connected to the two all metal angle valves through two bellows. The diaphragm pump can be switched on in any pressure range. It plays as a backing pump for the turbo. The starting pressure of turbo is below $10mbar$. But it is advisable to turn on turbo at pressure below $3mbar$. Turbo rotors will take a few minutes to reach full speed($1500s^{-1}$). Because of the extremely high rotation speed, the turbo must be properly fixed with aluminium profiles. The pressure of the whole chamber will take about half an hour to reach $10^{-6}mbar$ region after turbo reaches full speed.

It is necessary to do leak test before baking. The operation pressure of $RGA200$ is below $10^{-8}mbar$ for good sensitivity. Helium leak test is extremely sensitive since helium molecule is so small that it can easily penetrate through a small leak, it is also a totally dry test method. The sensitivity of the $RGA200$ can increase with the gain of the electron multiplier. The minimum detectable partial pressure limits as low as $10^{-12}mbar$.

After leak test, the system is then baked for four weeks. The different parts are baked at highest baking temperature individually by using several separately controlled heating tapes. Ion pumps also need to be fully baked without the magnets. The purpose of baking is to accelerate outgassing from inside surfaces of the vacuum chambers. In order to properly bake Zeeman tube(the Zeeman slower coil was already installed), a heating wire is wound directly onto it. During the baking procedure, it is important to make sure temperature gradients in time and space within the ranges allowed for the different components. Thermocouples are used to monitor different temperature.

3.5 Initialization of Ion Gauge and Ion Pump

At the end of the baking procedure, initialization of ion gauge and ion pump had to be done, since the initialization will produce large amount of gas and dirts, we hope these can be pumped out by turbo pump. Our initialization procedure is the following:

•Ion gauge initialization:

① Remove aluminium foil around the ion gauge.

② Decrease the temperature of ion gauge to 200℃ by Variac.

③ Write down the pressure in full range gauge(Pfeiffer PKR261) which measures the pressure of the whole vacuum chamber.

④ Install the ion gauge cable, then turn on the ion gauge.

⑤ Monitor the pressure in full range gauge. The value will shoot up and decrease, finally reach the same value recorded in step ③. Degas filament1 when the pressure is below $10^{-5}mbar$. It takes nearly 30 minutes for degassing. Write down the pressure after degassing. Turn off filament1.

⑥ Degas filament2 with the same steps for filament1.

⑦ Switch off the controller(Varian XGS-600).

•Ion pump initialization:

① Decrease the ion pump temperature to 150℃ by Variac.

② Write down the pressure in the full range gauge.

③ Further cool down the ion pump to room temperature. Remove the aluminium foil and the heating tapes on the ion pump.

④ Reinstall the magnets, wrap the heating tapes on the ion pump(with magnets) and fix thermocouple on it. Cover it with aluminium foil. Connect the high voltage cable to the ion pump controller(Varian MiniVac).

⑤ Increase the ion pump temperature to 150℃ by Variac.

⑥ When the pressure is below $10^{-6}mbar$ in the full range gauge, start the ion pump. Then wait till the pressure reaches the value recorded in step ②.

⑦ Switch off the ion pump and follow the same steps to initialize another ion pump.

After initialization of ion gauge and ion pumps, we can turn them on. Monitor the front display of the MiniVac controller. The ion pump current should rise and then fall. The pressure will quickly drop from $10^{-8}mbar$ to $10^{-10}mbar$. Gradually cooling the whole system to room temperature. Closing the all metal valves with a torque wrench($21Nm$). One day later, $7.5 \times 10^{-11}mbar$ was achieved in our experiment. Finally removing the roughing pump stage, the vacuum system is completed.

4. Laser System

This chapter discusses Laser system. The laser system is more or less developed from scratch. The layout of 671nm laser system for ^6Li red MOT in our experiment is shown in Fig(4.1). Cold atom experiments require laser beams for different purposes: slowing, magneto-optical trapping, repumping and imaging. A compact, flexible and reliable laser system is designed and built. In order to reach longer locking time and better power stability, the system is continuously improved throughout the apparatus construction.

The basic procedure of creating ^6Li MOT is the following: (1)Lithium chunk is heated in oven to produce lithium vapor; (2)the atomic beam is formed by lithium vapor effusing out of oven; (3)the atomic beam is slowed down by Zeeman shower; (4)the slowed atoms are captured by MOT.

4.1 Energy Level of ^6Li

The atomic energy levels of ^6Li atom is depicted in Fig(4.2).

Although MOTs can be created by using D1 line[29], D2 transition is usually preferred due to the higher transition strength and the almost closed cooling cycle for the trapping transition.

The peculiarity of ^6Li energy level structure is that the hyperfine structure in $2^2P_{3/2}$, the excited state of the trapping transition is unresolved, e.g. the hyperfine splitting of the excited state is on the order of the linewidth of the D2 transition. This property leads to significant consequences.

First, it makes polarization gradient cooling inefficient for lithium and results in a considerably higher temperature($\sim 300\mu K$)[30] of the laser-cooled atomic cloud compared to other alkali species.

Second, the cycling transition cannot be addressed individually. In a MOT, this results in comparable populations of the two ground states. Consequently, the repumping light with a similar detuning and intensity as the MOT trapping light is necessary. The

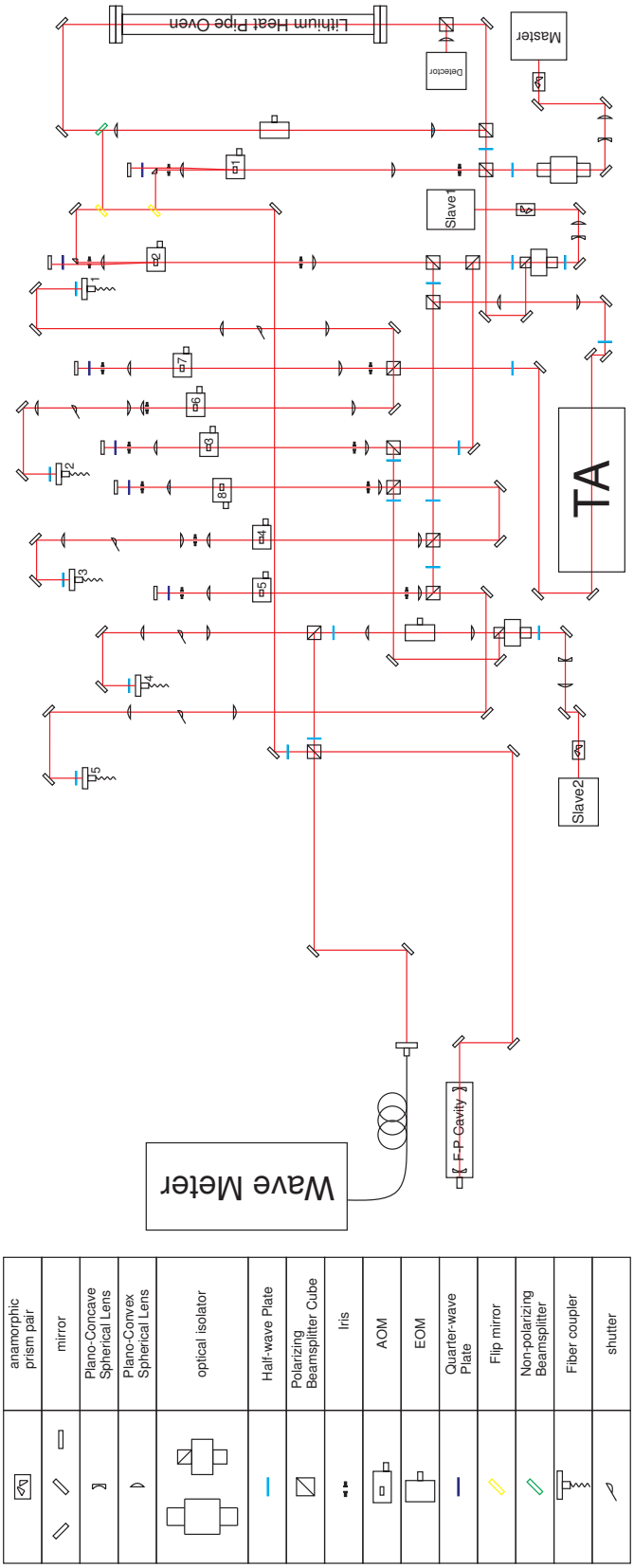

Figure 4.1: The layout of the 671nm laser system. Using prisms and flip mirrors couple laser beams into wave meter and Fabry-Perot(FP) cavity, the wavelength and spectral structure of all the lasers can be easily measured.

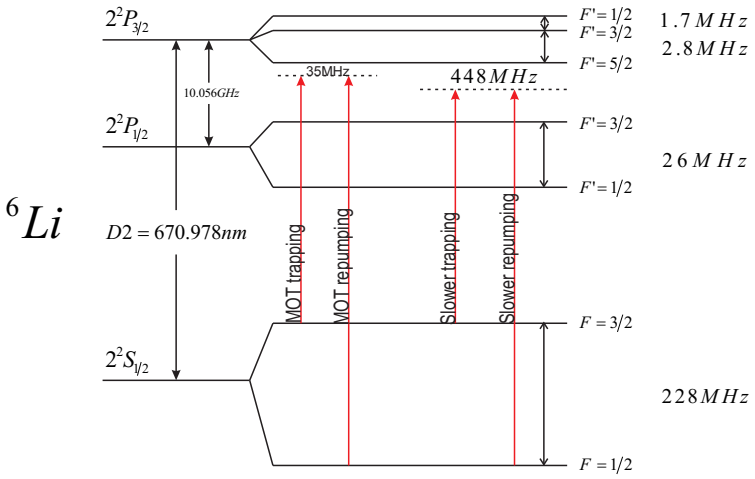

Figure 4.2: Energy level scheme for ^6Li atom. Red arrows indicate the optical transitions employed in the experiment.

same is true for the far red-detuned pair of trapping and repumping light used in the Zeeman slower.

4.2 Lithium Laser System

A schematic plot of the lithium laser system is given in Fig(4.3). As can be seen, one master laser, two slave lasers and one tamper amplifier(TA) laser are employed in this system. A master-slave scheme based on injection locking provides sufficient power for the experiment.

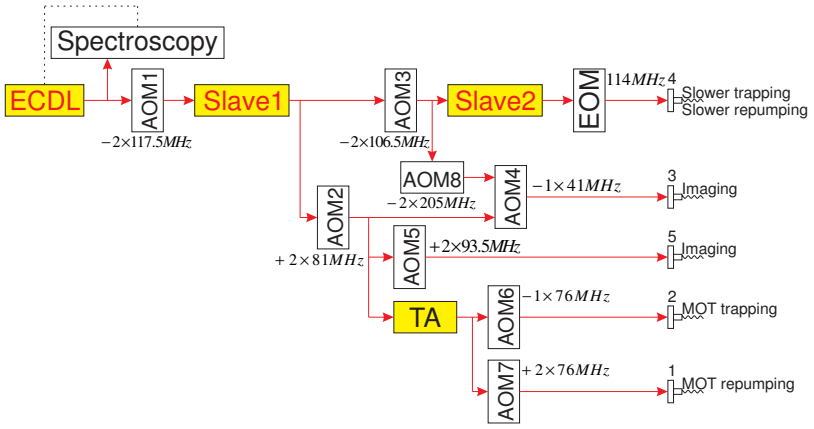

Figure 4.3: Block diagram for ^6Li laser system. Master laser is locked to spectroscopy signal. Slave1, Slave2 and TA are locked by injection locking. Slave2 works as a Zeeman slower laser. TA applies sufficient power for the MOT.

The beam from home made master laser is divided into two branches. The frequency of the master laser is locked to the cross-over of atomic transitions $|2^2S_{1/2}, F = 1/2\rangle \rightarrow$

$|2^2P_{3/2}\rangle$ and $|2^2S_{1/2}, F = 3/2\rangle \rightarrow |2^2P_{3/2}\rangle$. After AOM double pass configuration the frequency shifted experimental beam injects Slave laser1.

Slave laser1 is used to inject TA and Slaver laser2 as well as create imaging beams. The imaging beams resonate with the corresponding atomic transitions(imaging beam 3 resonates with transition $|2^2S_{1/2}, F = 3/2\rangle \rightarrow |2^2P_{3/2}\rangle$ and imaging beam 5 resonates with transition $|2^2S_{1/2}, F = 1/2\rangle \rightarrow |2^2P_{3/2}\rangle$).

MOT trapping beam is $-35MHz$ detuning from $|2^2S_{1/2}, F = 3/2\rangle \rightarrow |2^2P_{3/2}, F = 5/2\rangle$ transition, the same detuning from $|2^2S_{1/2}, F = 1/2\rangle \rightarrow |2^2P_{3/2}, F = 3/2\rangle$ transition for MOT repumping beam. The MOT beams come from TA have enough power for cooling and trapping lithium atoms.

Slave laser2 is the laser for Zeeman slower beams. Far red detuning($-448MHz$) are chosen for slower trapping and slower repumping beams.

To generate these frequencies, 8 AOMs[1] and 2 EOMs[2] are employed in this system. The height of laser beams is set to $3inches$ which gives best mechanical stability and good flexibility for alignment.

4.3 Frequency Locking of Master Laser

4.3.1 Home Made Master Laser

The master laser is built in Littrow configuration consisting of a laser diode[3], a collimator and a holographic diffractive grating[4]. The first diffraction order of the grating is reflected back into the laser diode to form the frequency selective external cavity. The zeroth order reflection from the grating serves as the output beam. The larger length of the external cavity which between the optical grating and the back facet of the laser diode reduces the linewidth of the diodes from about $50MHz$ to below $1MHz$. The mechanical structure of our master laser presented in Fig(4.4) follows the design suggested by Ref[31]. Mode hopping-free range can reach $9GHz$ by using feed forward configuration. The power of master laser measured after optical isolator is $17.5mW$[5].

[1] Gooch Housego; IntraAction
[2] New focus
[3] Toptica LD-0670-0025-AR-2, $25mw$ output power
[4] Thorlabs GH13-18V
[5] Newport power meter 1918-C

$60dB$ two stage optical isolator(Linos DLI2) can effectively block back reflections from surfaces of optical elements.

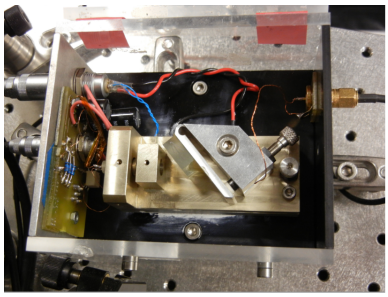

(a) The mechanical structure of master laser.

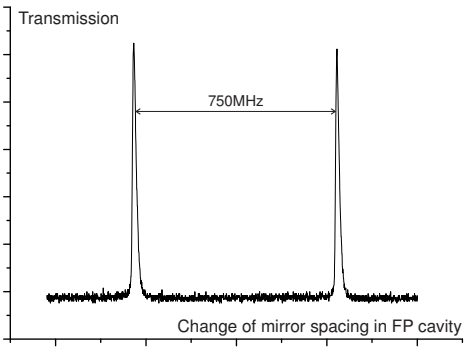

(b) The single mode spectrum of master laser.

Figure 4.4: Master laser. (a)Littrow configuration home made master laser. (b)The single mode spectrum of master laser observed in oscilloscope by scanning monitor FP cavity. The free spectrum range of the FP cavity is $750MHz$.

Due to the large beam divergence($parallel \approx 10°; perpendicular \approx 30°$) of the laser diode, we find only collimator from Optima Precision Inc.(336-1027-660) can well collimate the beam after trying a number of other collimators. Anamorphic prism pair is inserted into the beam path of master laser to shape the beam profile. A nearly circular beam is gotten after anamorphic prism pair. The diameter of the master laser beam is around $4mm$. The beam size is further reduced to $2mm$ by a compressing telescope with two lenses($100mm$, $-50mm$) in order to optimise the double pass efficiency of the first AOM.

4.3.2 Heat Pipe Oven

The atomic transition spectroscopy is considered as a frequency reference for the master laser. However, it is more difficult to construct a vapor cell for spectroscopy of lithium compare to other alkali elements(Cs, Rb, K) due to the low vapour pressure at room temperature[32]. Lithium has to be heated to more than 300℃ to reach the required optical density.

We have built a heat pipe oven[33, 34] for spectroscopy of lithium on the 671nm transition. A heat pipe oven continuously generates homogeneous vapor with well-defined temperature, pressure and optical density. The design of a heat pipe oven[35] is illustrated in Fig(4.5).

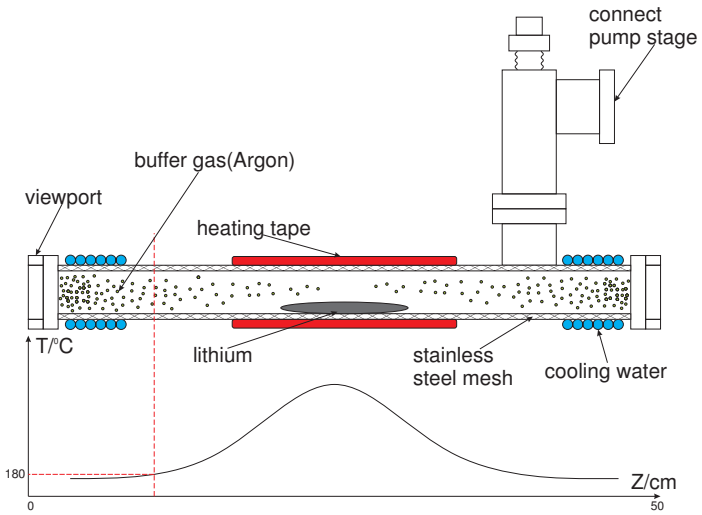

Figure 4.5: Schematic diagram of a heat pipe oven. Full metal angle valve provide the access to pump the tube and fill argon. The temperature gradient is created along the tube, lithium is recycled through the mesh.

It consists of a 50cm long stainless steel tube whose two ends are closed by uncoated CF40 commercial viewports[6]. The tube is pumped through a full metal angle valve[7]. Lithium chunks locate in the middle of the tube are heated by a heating tape. The temperature of the heating tape can be controlled by Variac and monitored by thermocouple. The heat isolation material wrapped heating tape increases the heating efficiency. Stainless steel mesh can be considered as a capillary structure on the inner surface of the tube. The vapour gas is confined by the buffer gas(UHP Argon) which prevent the vapor from condensing on the viewports. The temperature gradient along the tube is created by the cooling water. The operating temperature of our heat pipe oven is 300℃, when the temperature beyond the melting point of lithium(180℃), lithium chunks start melting down and wetting the mesh. The higher temperature in the center will cause the vapor diffuse towards two ends to push the buffer gas. Because of the cooling water, the temperature below melting point at two ends of the tube. So the vapor condensates. The condensate returns through the wick of mesh back to the center by capillary action. Finally equilibrium will reach, in which the center part of the tube is filled with the lithium vapor at constant temperature and pressure.

The heat pipe oven has at least two significant advantages:

① The filled buffer gas limits the mean free path of the metal vapor so that it cannot reach and coat the viewports.

[6]Kurt J.Lesker
[7]Vacom GMV-40R

② The capillary structure and the temperature gradient allow the circle of vapor evaporation and condensation take places. Then continuous operation is possible.

To build such a heat pipe oven, the components should be properly cleaned first. Then carefully assembling and putting the metal mess in. One week prebaking and pumping can remove most of water and other dirts. Lithium is prepared follow the same procedure described in 3.3. Variable leak valve[8] can precisely control the flux of UPH Argon. Open one of the viewports and quickly load lithium. Then seal the viewport again. Another week of baking and pumping is needed to remove the water, oil and other dirts from lithium chunks. Finally cooling the whole system down to room temperature. $10^{-8}mbar$(full metal valve open) and $10^{-6}mbar$(full metal valve closed) is achieved. The amount of buffer gas is decided by the absorption signal. Filling Argon till the signal becomes broadening because of collision between lithium and buffer gas. About $1.3 \times 10^{-3}mbar$ Argon is filled in our heat pipe oven.

4.3.3 Doppler-free Saturated Absorption Spectroscopy

The technique of Doppler-free saturated absorption spectroscopy is frequently used as a tool for locking the lasers to particular atomic lines. A good review article of Doppler-free spectroscopy technique was written by T. W. Hänsch, A. L. Schawlow, and G. W. Series[36].

① Doppler broadening of spectral lines

Because of the Doppler effect, atoms moving with velocity $\vec{v}$ absorb radiation when laser detuning $\delta = \omega - \omega_0 = -\vec{k}\cdot\vec{v}$. Where the wave vector of the radiation has magnitude $k = \omega/c = 2\pi/\lambda$. Thus

$$\frac{\delta}{\omega_0} = \frac{v}{c} \tag{4.1}$$

Substituted this into MD distribution. The absorption has the Gaussian line shape function

$$g_D(\omega) = \frac{c}{v_{mp}\omega_0\sqrt{\pi}} exp\left[-\frac{c^2}{v_{mp}^2}\left(\frac{\omega-\omega_0}{\omega_0}\right)^2\right] \tag{4.2}$$

The Doppler-broaden line has a full width at half maximum of $2\sqrt{ln2}\frac{v_{mp}}{c}\omega_0$. The width is about $178.8MHz$ for ^6Li.

[8] Varian

② Saturated absorption spectroscopy

Saturated absorption spectroscopy(Fig4.6) is one of the most common techniques to get Doppler free signal. The beam splitter divides the power of the laser beam between a weak probe($1mW$) and a stronger pump beam($10mW$). Both beams have the same frequency ω and go in opposite directions through the heat pipe oven.

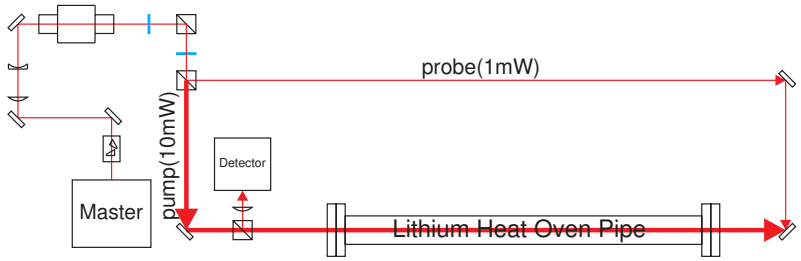

Figure 4.6: Saturated absorption spectroscopy.

When the laser has a frequency far from resonance, $\mid \omega - \omega_0 \mid \gg \Delta\omega_{hole}$, the pump and probe beams interact with different atoms so the pump beam does not affect the probe beam. Close to resonance, $\omega \approx \omega_0$, both beams interact with atoms in the velocity class with $v \approx 0$, and the hole burnt by the pump beam reduces the absorption of the probe beam. Thus saturation of the absorption by the pump beam leads to a narrow peak(hyperfine structure) in the intensity of the probe beam transmitted through the sample. Fig(4.7) shows a zoom in look of the hyperfine structure of the ^6Li D2 line.

$$\Delta\omega_{hole} = \Gamma\left(1 + \frac{I_{probe}}{I_{sat}}\right)^{1/2} \tag{4.3}$$

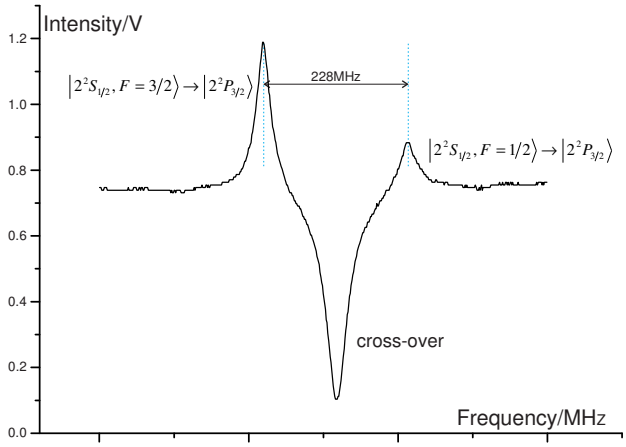

Figure 4.7: Hyperfine structure of ^6Li D2 transition. Except two real transition peaks, a so called cross-over peak appears in the middle of them. In our case $\lambda = 670.978nm$, $I_{probe} = 1mW$, $\Delta\omega_{hole} = 21MHz$. Heat pipe oven with $1.3 \times 10^{-3}mbar$ Argon is heated at 300℃.

③ Cross-over resonance

The real atoms have multi-level structure. If two atomic transitions with a common lower or upper level overlap within their Doppler width, extra resonances, called cross-over resonances, occur in the saturation spectroscopy(Fig4.8).

Assume that for the resonance frequencies ω_1 and ω_2 of the two transitions, $\mid \omega_1 - \omega_2 \mid < \Delta\omega_D$ holds. When the laser frequency $\omega = (\omega_1 + \omega_2)/2$. In the case of a common lower level, a group of atoms with velocity $\vec{v}$ are saturated by the pump beam, leads to a decrease of the population in the common lower level. So the probe beam on another transition goes through the atom sample nearly without absorption, which result in a saturated cross-over peak. In the case of a common upper level, the pump beam pumps atoms into another lower level through the common upper level. Therefore the absorption of probe beam is enhanced, which result in a enhanced cross-over peak.

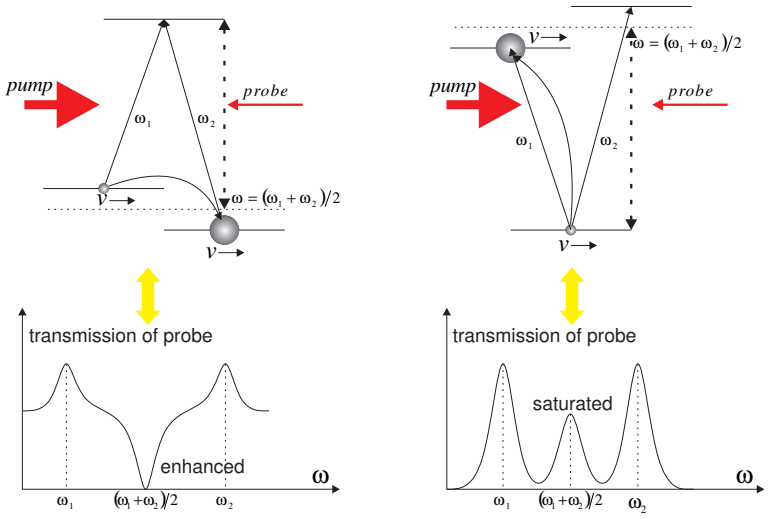

Figure 4.8: Cross-over peak. Cross-over peaks appear between two real atomic transitions. The direction of cross-over peak depends on Λ or V type energy level configuration. There is no cross-over in the middle of two cross-over peaks.

4.3.4 Frequency Modulation(FM) Spectroscopy

Although free running external cavity diode laser has a narrow linewidth(in the MHz range) and small drift (in the 10s of MHz to GHz range[9]), cold atom experiment demands more precise control. Laser locking can eliminate laser drifts and with modern locking electronics, linewidths of diode lasers can be reduced to kHz range and even below $1Hz$ [37].

[9]Diode Laser Locking and Linewidth Narrowing Rudolf Neuhaus, Ph.D. TOPTICA Photonics AG

In order to lock the laser on the top of the atomic transition line. We make a arrangement of FM spectroscopy configuration(Fig4.9). FM spectroscopy is a method of optical heterodyne spectroscopy capable of sensitive and rapid detection of absorption or dispersion features[38].

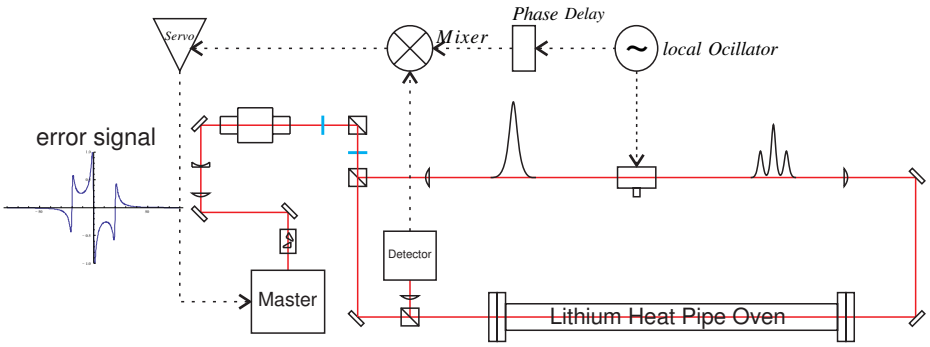

Figure 4.9: Experimental arrangement for FM spectroscopy. The error signal guides electro-servo loop to lock the laser frequency.

The probe beam $E_{probe} = E_0 e^{i\omega_0 t}$ is phase modulated by EOM. Two sidebands are added to the carrier after the EOM:

$$E_{probe} = E_0 e^{i(\omega_0 t + \beta sin(\Omega t))} \approx E_0 \left\{ e^{i\omega_0 t} + \frac{2}{\beta} e^{i(\omega_0+\Omega)t} - \frac{2}{\beta} e^{i(\omega_0-\Omega)t} \right\} \tag{4.4}$$

They are out of phase. For small modulation index β(i.e. $\beta << 1$), the carrier and first order sidebands contain nearly all of the power.

The beam is then passed through the lithium heat pipe oven. It is convenient to define the amplitude attenuation δ and optical phase shift ϕ for each spectral component, the transmitted field is

$$E(t) = E_0 \left\{ e^{-\delta_0 - i\phi_0} e^{i\omega_0 t} + \frac{\beta}{2} e^{-\delta_{+1} - i\phi_{+1}} e^{i(\omega_0+\Omega)t} - \frac{\beta}{2} e^{-\delta_{-1} - i\phi_{-1}} e^{i(\omega_0-\Omega)t} \right\} \tag{4.5}$$

The detected electrical signal is proportional to $I(t)$:

$$I(t) = C|E(t)|^2 = C\left[1 + (\delta_{-1} - \delta_{+1})\,\beta cos\Omega t + (\phi_{+1} + \phi_{-1} - 2\phi_0)\,\beta sin\Omega t\right] \tag{4.6}$$

The $cos\Omega t$ component of the beat signal is proportional to the difference in amplitude loss experienced by the upper and lower sidebands, whereas the $sin\Omega t$ component is proportional to the difference between the phase shift experienced by the carrier and

the average of the phase shifts experienced by the sidebands.

On resonance, these two beats will be 180° out of phase with respect to each other due to the nature of FM. Therefore the two beats will exactly cancel and this zero point used as the locking point which guides the electro servo loop to lock the laser frequency to the atomic resonance transition. The error signal gained in this FM spectroscopy setup is presented in Fig(4.10)

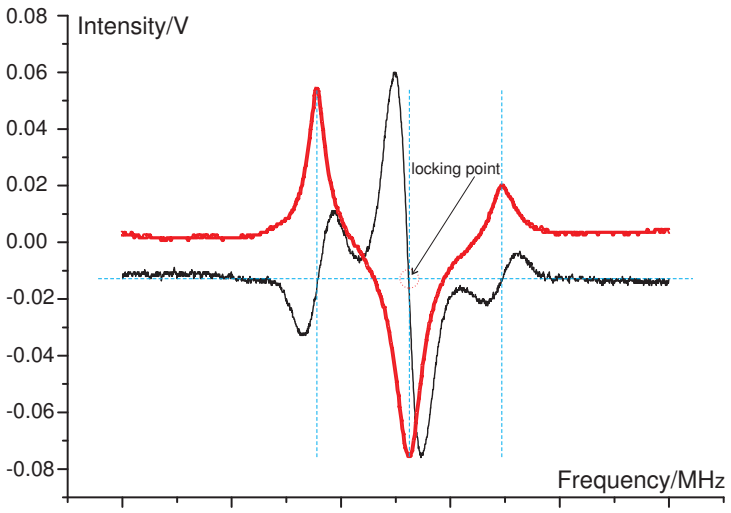

Figure 4.10: Error signal for ^6Li D2 transition. Modulation frequency of the EOM is $32MHz$. Heat pipe oven with $1.3 \times 10^{-3} mbar$ Argon is heated at 300℃. The red curve is the hyperfine structure of the ^6Li D2 transition.

4.4 AOM Double-pass Configuration

Acousto-optic modulators(AOMs) are widely used elements in laser cooling experiments for the frequency control. The laser frequency can be scanned by scanning the AOM driving frequency. In this case, however, the deflection angle of the ±1 order beam shifts as well since it is a function of the driving frequency. Changes in the laser propagation direction is usually an unwanted side effect. AOM double-pass configuration can effectively eliminate this change during frequency sweeps[39]. The schematic diagram of AOM double pass configuration is shown in Fig(4.11).

The output of the ±1 order of the AOM is retroflected for a second pass through the AOM leading to a frequency shift of $2\Delta f$ on the double passed beam. In this configuration, scanning the driving frequency(Δf) of the AOM does not change the propagation direction of the double passed beam due to the second lens. A $\lambda/4$ wave

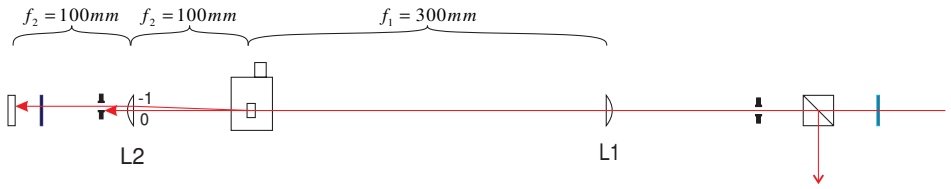

Figure 4.11: AOM double pass configuration.

plate placed before the retroflector causes the retroflected beam to have polarization orthogonal to that of the incident beam. A polarizing beam splitter is placed to separate these two beams.

To align the double pass AOM configuration:

① Make sure the beam is horizontal and goes straight through the center of the polarizing beam splitter cube. This can be done with the help of two irises.

② Position lens 1 such that the beam passes through the center of the lens.

③ Position the mounted AOM(Thorlabs KM100P/M) at the beam focus. The position of the focus point can be determined by beam master[10] or by knife-edge measurement. Then turn on AOM, select first order with an iris, optimize single pass efficiency by tweaking around AOM.

④ Position lens 2. Insert lens 2 at its focal length from the AOM. Turn off the AOM , let the beam goes through the center of the lens.

⑤ Put reflector(Newport U100-A2K) at the focal length from the lens 2 and insert $\lambda/4$ waveplates in front of the reflector. Turn on AOM again, overlap the reflected beam and incident beam. Place a power-meter after the cube and maximum the power of double passed beam by tuning the reflector and rotating the $\lambda/4$ waveplate(put another iris before the cube to select double passed beam).

⑥ Optimize the position of lens 2. Scanning AOM driving frequency, slight move the lens back and forth to minimum the position change of double passed beam at far distance downstream. A better method is that coupling the double passed beam into optical fiber, minimum the output power change of the fiber.

For all the AOMs used in the laser system, the single pass efficiency and double pass efficiency are listed in the Table(4.1).

[10] Coherent BeamMaster BM-3 Silicon-UV Detector Head

AOM	Single-pass	Double-pass
1	82.7%	71.1%
2	83%	62.9%
3	77.4%	61.4%
4	83.8%	
5	81.5%	62%
6	84%	
7	82.7%	65.4%
8	83%	57%

Table 4.1: Measurements of AOM efficiency(refer to Fig 4.1).

4.5 Injection Slave Laser and TA

① Slave laser

The laser diode[11] is specified with an output power of $120mW$ and a free running wavelength of $661nm$ at 25℃. Because temperature tuning can cover a frequency range of the order of several tens of nm at a typical rate of $0.3nm/K$. To run slave lasers at $671nm$ the laser diodes are heated to about 70℃ and operated at a current above the specifications to reach the desired sufficient power.

The laser diode has small beam divergence($parallel \approx 10°; perpendicular \approx 17°$) which can be well collimated by Thorlabs collimation tube(LT230P-B). The beam profile is also shaped by anamorphic prism pair. The diameter of the slave laser beam is around 2mm. Mode matching with master laser is done by a expansion lens telescope. Two stable mirror mounts with fine screw thread[12] are used to couple the injection beam into slave laser(Fig4.12).

Injection locking utilises the frequency effects that a harmonic oscillator can be captured by a second oscillator when the coupling is strong enough and the frequencies near enough, the captured(locked) oscillator has essentially identical frequency as the second.

In order to lock the slave laser to master laser. First, carefully overlap injection beam and leaking beam of slave laser from the injection port of optical isolator[13]. Giving enough power to the injection beam($1mW$ is a good starting value). Setting the current value of slave laser at where the output power is large enough. In experiment, we set

[11] Mitsubishi, ML101J27
[12] Newport U100-A2K: 100TPI thread
[13] OFR IO-5-671-PBS

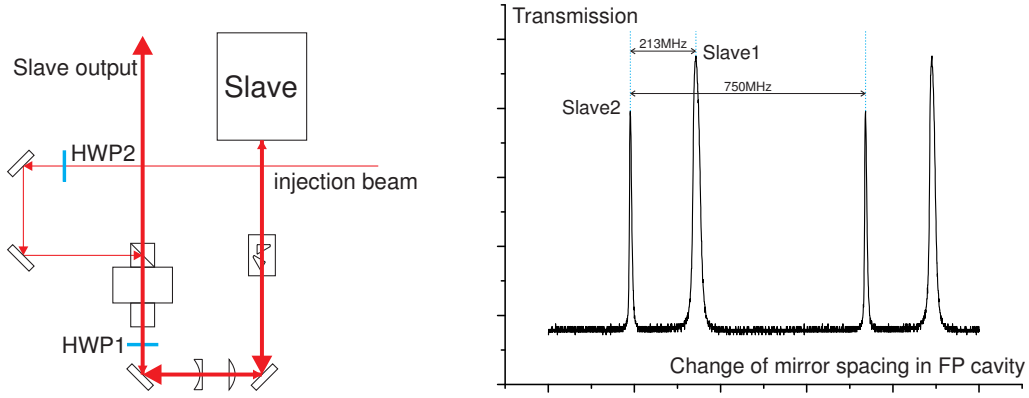

(a) Injection locking configuration. **(b)** The spectrum of slave lasers.

Figure 4.12: Injection locking of slave lasers. (a)Half wave plate(HWP) 1 is used to optimism the transmission of the optical isolator. HWP2 is used to optimism the seeding. (b)The spectrum of locked slave1 and slave2. The frequency of slave2 is shift $-213MHz$ from slave1 by AOM double pass configuration.

this value around $310mA$. Coupling the beam from slave laser into FP cavity. Then increase the temperature of slave laser, monitor the spectral structure of the slave laser. As the temperature changes, the spectral structure changes dramatically. However, the slave laser can be locked at several temperature points. Then set the temperature at these values, slightly change the current and fine tune coupling mirrors to make lock stable. Reducing the power of injection beam, slightly change the current and tweak mirrors again. Try different temperature and iterate these procedures to optimise the injection locking(using the smallest injection power to achieve stable locking).

Our two slave lasers continuously ran for nearly half an year without degradation. Stable locking of two slave lasers has been obtained with the injection power around $200\mu W$. Typical output power for the slave lasers after the optical isolator are more than $80mW$.

② Tapered Amplifier

Tapered amplifier(TA) diode[14] offers sufficient power for the MOT trapping and repumping beams. According to the data sheet, the maximum output power is $500mW$ at operating temperature of 20℃. The injection wavelength is $670nm$ and maximum injection power is $24mW$.

A compact TA box is built which contains a special designed brass base for the TA chip and two collimation lens, a rail which fix the position of $60dB$ optical isolator and a plano-convex cylindrical lens.

[14]Toptica TA-0670-0500-6

The TA chip is fixed on the brass base, and the temperature of the chip is controlled by a TEC element which conduct with the bottom of the base. When the TA chip running, there are two laser beams emit forward and backward, respectively. First, collimate the backward beam with a suitable collimator. Coupling the seeding beam into TA chip is done by overlapping the seeding beam with this backwards beam using a pair of mirrors. Carefully choosing a lens telescope to optimise mode-matching will improve the coupling efficiency. The plane of the tapered gain element is horizontally oriented, when seeding light feeds into the gain element, avalanche amplification of photos occurs, the tapered shape is designed to dilute the energy density so that prevent burning the chip from huge amount of energy. Therefore, the TA should be avoid any reflected light, because even small amount of light will be amplified in the backward direction and heat will accumulate due to the small area. So TA chip can be easily destroyed. An output collimator with large numerical aperture is used and position a $60dB$ optical isolator to maximum the output power. During the alignment of TA, carefully avoid blocking beam between output collimator and optical isolator. Since the plane of the tapered gain element is horizontally oriented, the diffraction yields a large vertical divergence. The output collimator only collimates the beam in vertical direction, but yields a focus in the horizontal plane. We compensated the astigmatism of the beam with a plano-convex cylindrical lens after optical isolator[40]. The astigmatism correction is shown in Fig(4.13). We run TA at output power of $260mW$(measured after optical isolator).

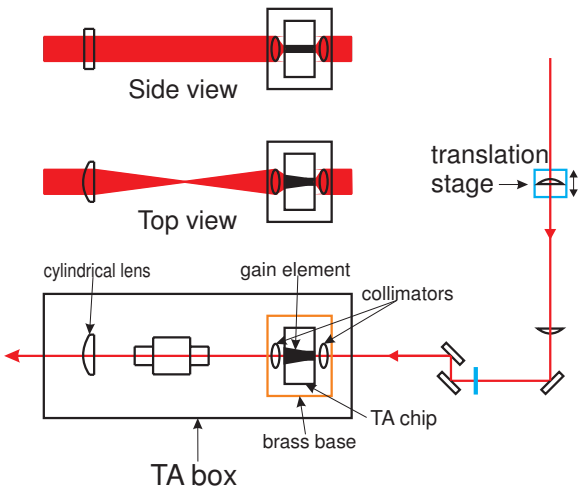

Figure 4.13: Schematic of injecting TA and astigmatism compensation. Translation stage(OWIS MT 45-13-X-MS) allows to precisely control the mode-matching lens telescope. HWP matches the polarization between seeding beam and TA beam. A plano-convex cylindrical lens compensates the astigmatism.

4.6 Fiber Coupling

All the beams(MOT trapping and repumping, imaging, slower trapping and repumping) can be created in this laser system with precise frequency and enough power. In order to slow, trap, image and manipulate atoms, these beams are finally coupled into optical fibers and transmitted to vacuum table. Optical fibers are not only waveguides that can transport optical energy and information but also modes filters that can filter out bad modes and give very good Gaussian mode.

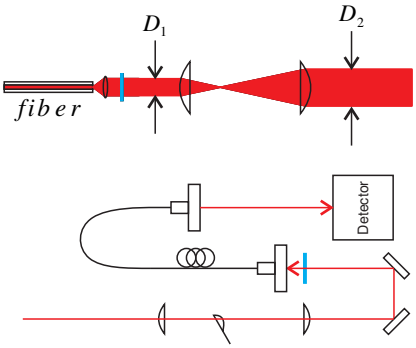

Figure 4.14: Fiber coupling. Fast photodetector is more sensitive than power meter. It makes easier to optimize the coupling.

Once the beam leaves the fiber, however, without confinement the beam begins to spread. The diverged beam can be collimated by a collimator[15]. The diameter of the collimated beam is D_1. To do a efficient fiber coupling, the reversed process can be considered. As shown in Fig(4.14), the injection beam is collimated and whose diameter is D_2, which is usually not equal to D_1. To match them we choose a telescope system according to the ratio of D_1/D_2. A mechanical shutter locates at the focal point of the telescope system. It can quickly shut down the beam. Two stable and fine adjustment mirror mounts are used to couple the beam. To optimize the output, it is suggested that measure the output light intensity with a fast photodetector. Rotate $\lambda/2$ waveplate before the fiber input to minimum the polarization fluctuation till there is almost no power fluctuation of the output beam when you slightly bent or warmed fiber by hand.

Table(4.2) specifies the coupling efficiencies of all the fibers used in laser system.

[15]Thorlabs C230TME-B

Fiber	Function	Coupling
1	MOT repumping	75.1%
2	MOT trapping	78%
3	Imaging	62.9%|63.6%
4	Slower	65%
5	Imaging	62.5%

Table 4.2: Fiber coupling efficiency. For Fiber 3, 62.9% and 63.6% correspond to low field and high field(Feshbach coil) imaging, respectively.

5. Red MOT and Characterization

This chapter reports the attempts of creating the red MOT. The operation procedures and working conditions are discussed. Detailed measurements of the MOT have not been completed since Labview control programme is not yet finished.

5.1 MOT Optics

Two types of optical fibers are used in the laser system. A commercial fiber cluster device(Evanescent Optics Inc.) which has two inputs and six outputs is chosen for MOT trapping and repumping beams. The schematic figure is shown in Fig(5.1). The device simplifies the MOT optic setup a lot. The MOT trapping and repumping beams are coupled into two inputs, respectively. These two beams then mixed together and evenly distributed into six outputs. The fiber coupling efficiency is around 80%. For the imaging and slower beam, we use home made fibers[1]. The coupling efficiency of home made fiber is more than 60%.

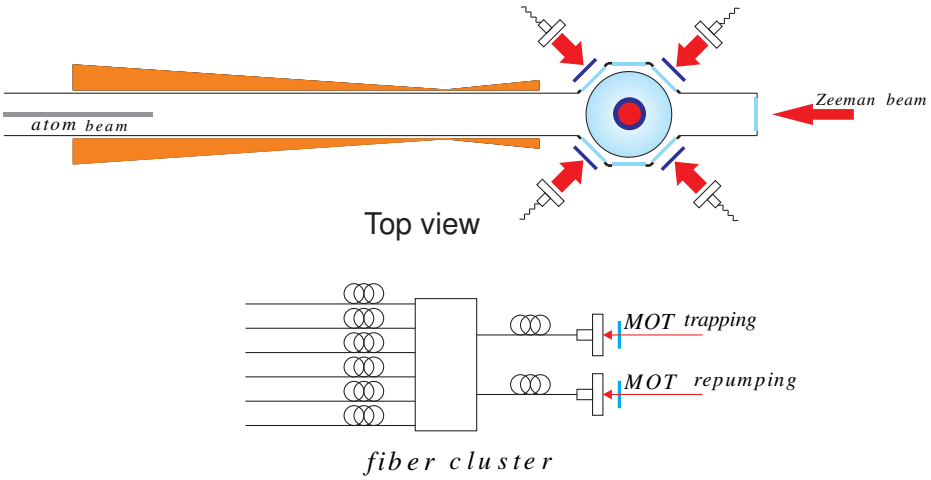

Figure 5.1: MOT optics. It contains six cage systems and $\lambda/4$ waveplates. Using cage systems to couple six laser beams into MOT chamber along the Cartesian axes. Six $\lambda/4$ waveplates can change polarization of each beams.

Cage systems are designed and built for the six output ends of the commercial fiber cluster device. The six fiber heads can be easily plugged in and removed from the cage

[1]Newport

systems. The function of the cage system is to expand and collimate the output beam of the fiber. Two fine thread screws let us can easily couple the collimated beam into the MOT chamber to capture the atoms. The cage system not only has good mechanical stability but also make the MOT optics more compact.

Cage system consists of two achromatic doublet lenses[2], $\lambda/2$ waveplate and PBS are used to collimate and expand the output beam from the commercial fiber cluster. An adaptor plate fixes two achromatic lenses with different size. This design also improves stability. The beam waists of the collimated beams are aimed at around $10mm$. The realised values are listed as below. The collimated MOT beams with linear polarization are finally translated to circular polarization beams by $\lambda/4$ waveplates in front of the MOT chamber windows. The four horizontal beams are set to σ^+ polarization, two vertical beams are set to σ^- polarization. The polarization direction of the laser beam should always reverse with the direction of MOT magnetic field. Carefully aligning the six MOT beams, overlap the counter-propagated beams and make sure the beam pass through the center of MOT chamber windows.

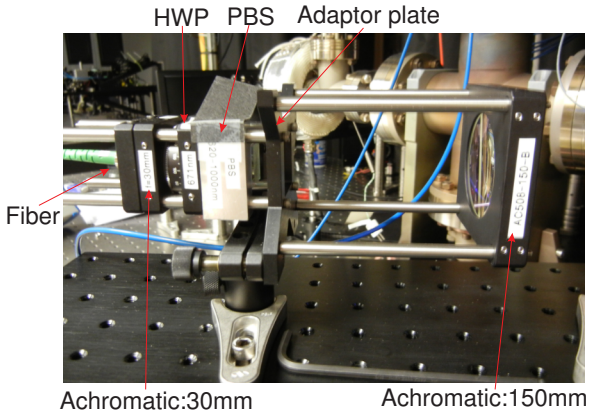

Figure 5.2: Cage system

Cage	Beam waist(ω_0)
1	8.88 mm
2	8.92 mm
3	8.98 mm
4	9.01 mm
5	8.95 mm
6	8.89 mm

Table 5.1: Beam waist

5.2 Red(671nm) MOT of ^6Li

To get the red MOT, we first set the values of Zeeman slower current and MOT current to $10A$ and $15A$, respectively. These designed values work as a starting point to the experiment. Increasing the oven temperature from 300℃ to 330℃, the oven nozzle temperature from 350℃ to 400℃. $13mW$ Zeeman slower beam with σ^- polarization effectively decrease atoms. The atoms can be blown back instead of reach the MOT

[2]Thorlabs AC254-030-B, AC508-150-B

chamber if the slower beam too strong. The power for each MOT beam are listed in Table 5.2.

After first get the MOT(It is quite small, likes a red spot.), optimising the MOT by balance the power between the counter-propagated beam pairs. Fine tuning the MOT beam alignment, rotating the $\lambda/4$ waveplates and changing the power of slower beam. The quite large MOT beam size and beam power allow to catch a reasonably large MOT. A roughly estimation by eye, the size of optimized MOT is about $1cm$. The lifetime of the MOT is about $40s$ by fluorescence Measurement.

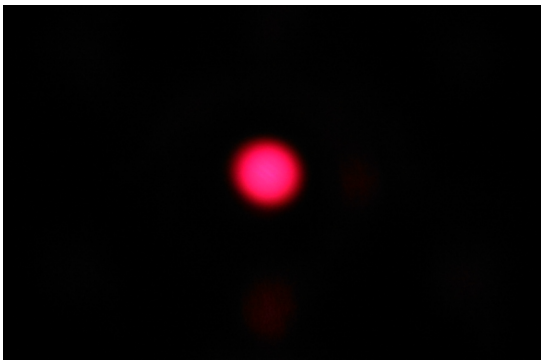

Figure 5.3: Red MOT of ^6Li

Cage	Trapping and repumping	Trapping
1	14.3mW	9.8mW
2	15.1mW	10mW
3	12.6mW	8.4mW
4	12.8mW	8.4mW
5	12.1mW	8.1mW
6	14.1mW	9.3mW

Table 5.2: Output power

6. UV Spectroscopy of ^6Li

To improve the loading efficiency from MOT into optical dipole trap, the ^6Li atoms should be cooled to μK region. The linewidth Γ of an atomic transition sets the lower limit of the Doppler cooling temperature when atoms are cooled with the corresponding laser light. The D2 transition in ^6Li leads to the Doppler temperature $T_D = 141\mu K$. In contrast, the linewidth of the UV transition($|2^2S_{1/2}\rangle \rightarrow |3^2P_{3/2}\rangle$) is seven times narrower than the D2 line(Table(6.1)). We attempt to produce the UV MOT of ^6Li using this narrow transition[41]. Similar to red(D2 transition) MOT, $|2^2S_{1/2}, F = 3/2\rangle \rightarrow |3^2P_{3/2}\rangle$ and $|2^2S_{1/2}, F = 1/2\rangle \rightarrow |3^2P_{3/2}\rangle$ are employed as trapping and repumping transition respectively in the UV MOT(Fig(6.1)). In order to achieve UV MOT, the laser frequency must be stabilised to $|2^2S_{1/2}\rangle \rightarrow |3^2P_{3/2}\rangle$ transition. Due to the relatively small transition strength[42], it is not a straightforward work. This chapter reports the UV Doppler free absorption signal and error signal.

Parameter	D2 transition($\|2^2S_{1/2}\rangle \rightarrow \|2^2P_{3/2}\rangle$)	UV transition($\|2^2S_{1/2}\rangle \rightarrow \|3^2P_{3/2}\rangle$)
λ	$670.978nm$	$323.361nm$
$\Gamma/2\pi$	$5.872MHz$	$764KHz$
T_D	$141\mu K$	$20\mu K$
T_R	$3.5\mu K$	$15\mu K$

Table 6.1: Temperature limits on D2 and UV transition of ^6Li.

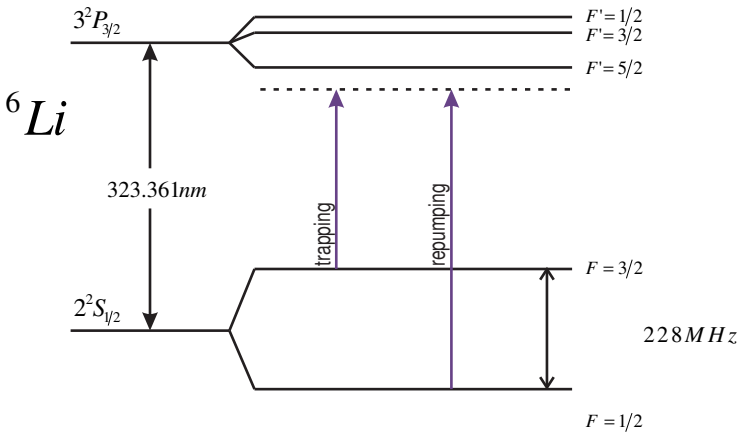

Figure 6.1: Energy level scheme on UV transition of ^6Li. Blue arrows indicate the optical transitions employed in UV cooling stage.

6.1 UV Spectroscopy Setup

We built another heat pipe oven for UV spectroscopy. The tube is much narrower and longer than the one for D2 transition due to the relatively small transition strength. Longer tube increases the interaction length between light and atoms, narrower tube confines the solid angle of lithium atoms impact viewport. This design will reduce the possibility of coating viewports by lithium atoms. Because the tube needs to be heated to nearly 400℃ to get usable signal, cooling water, metal mesh and buffer gas($5.3 \times 10^{-3} mbar$ Argon) are necessary which similar to the heat pipe oven for D2 transition.

Toptica SHG laser system is the UV source. The 646nm fundamental light from DL pro is amplified by a TA chip, then is seeded into a frequency doubling cavity. Finally, $39mW$ UV(323nm) light is available for the experiment. In the experiment, the doubling cavity is locked to the DL pro fundamental light to get maximum UV power. The fundamental light is locked to the Zerodur cavity by standard PDH locking technique to narrow down the linewidth. Therefore, the UV laser frequency can be scanned by scanning the cavity length of the Zerodur cavity. The corresponding locking scheme is shown in Fig(6.2). The UV Doppler free absorption signal is probed with this narrowed UV light in the optical setup which presented in Fig(6.3).

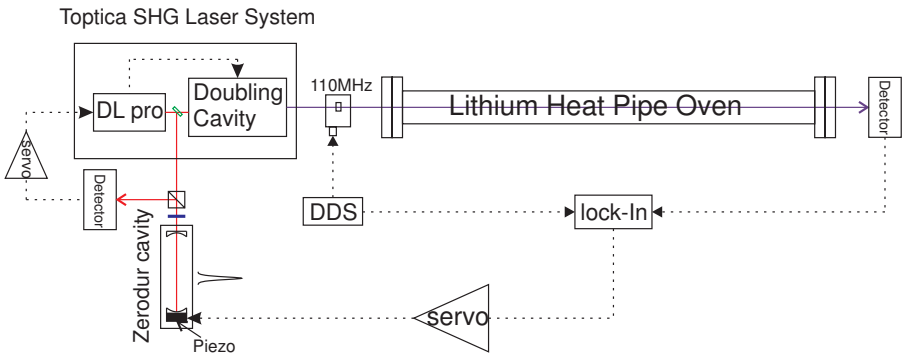

Figure 6.2: The locking loop of the UV laser. The Zerodur cavity has very good short term stability, Locking the fundamental light to the cavity is the fast locking loop. On the other hand, The absorption signal has very good long term stability. The long term frequency drift of the cavity is corrected by this slow locking loop.

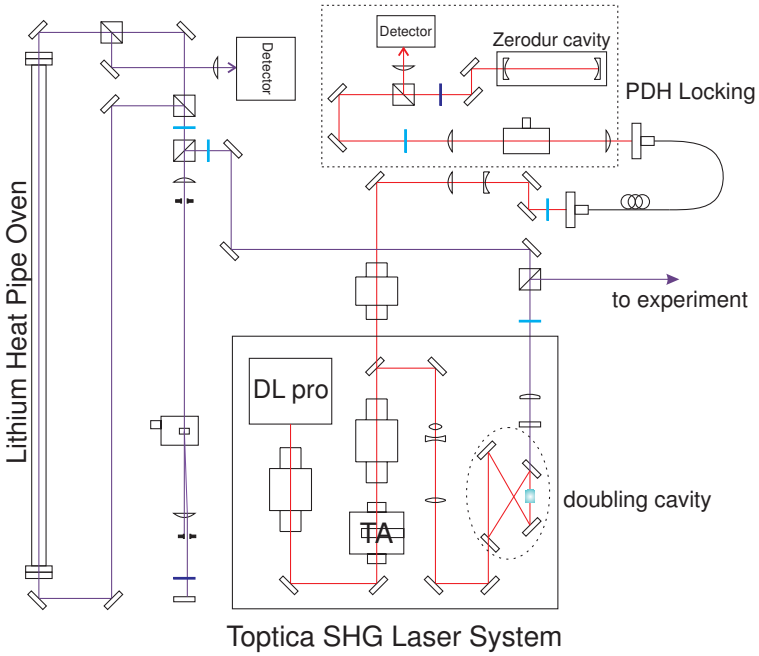

Figure 6.3: UV Spectroscopy Setup. The doubling cavity is locked to the fundamental light of the SHG Laser system. The fundamental light is locked to the Zerodur cavity to narrow the linewidth. The UV light frequency is modulated by the AOM for the lock-in detection. The Doppler free signal is detected in a saturated absorption configuration.

6.2 Lock-in Detection

The detector measures the weak UV probe beam transmitted through the heat pipe oven. The signal is too weak to detect directly. The whole signal is buried by the noise(Fig(6.4)[1]).

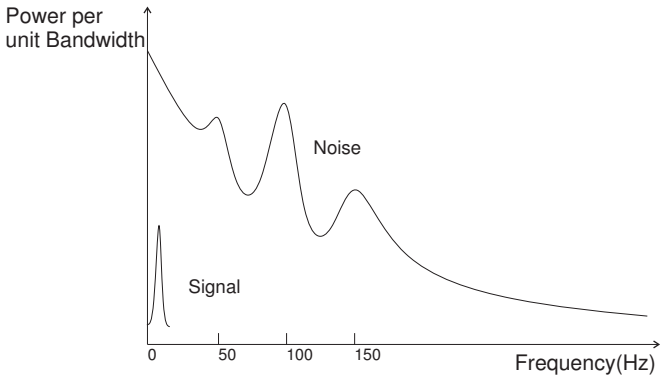

Figure 6.4: Distribution of noise and signal from the photo detector. The noise curve increases in the low frequency end and decreases in the high frequency end. The low frequency noise contains flicker noise associated with semiconductor devices, variations in dark current and variations in ambient light leaking into the detector. At higher frequencies the spectrum flattens out to give a reasonably constant shot noise background which is associated with the quantum nature of light.

The most noticeable feature of this curve is that noise power steady increases towards

[1]the curve is cited from the menu of Bentham Lock-in amplifier, Bentham Instruments Ltd

zero Hz. To significantly improve the signal to noise ratio, the signal information should be moved away from the high noise(low frequency) region. This can be completed by modulating(periodically interrupt) the UV light by an AOM[2] between the light source and the detector. Now the problem is that the signal is modulated(AC), i.e. its average value is zero. To record a value from the signal we must rectify it.

All the purposes can be done by Lock-in amplifiers. A lock-in amplifier provides a DC output proportional to the AC signal(in this case is the modulated UV light) under investigation. The heart of the lock-in amplifier is the phase sensitive detector(PSD), which is also known as a demodulator or mixer. All lock-in amplifiers rely on the concept of phase sensitive detection. Phase sensitive detection refers to the demodulation or rectification of an AC signal by a circuit which is controlled by a reference waveform derived from the device which caused the signal to be modulated. The phase sensitive detector only responds to signals which has the same frequency and phase with the reference waveform and rejects all others. Fig(6.5) shows the block diagram of a typical lock-in amplifier.

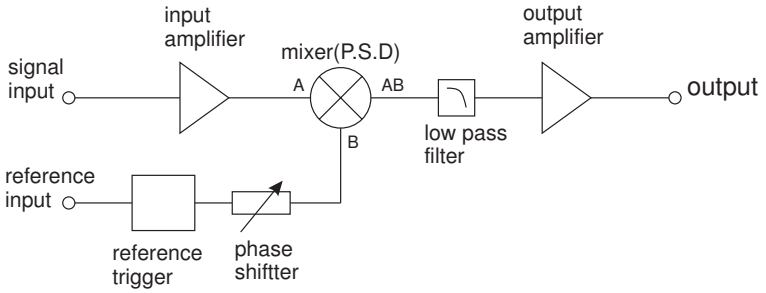

Figure 6.5: The schematic diagram of a lock-in amplifier.

In the signal input channel, the input signal, including noise, is amplified by an amplifier in order to match the optimum input signal range of the PSD. In the reference input channel, the reference signal is passed through a phase shifter, which is used to compensate for phase differences that may have been introduced between the signal and reference inputs by the experiment. The phase shifter is necessary since that proper operation of the PSD requires the generation of a precision reference signal within the instrument. The PSD multiplies the input signal with the reference signal. The purpose of the low pass filter is to remove the AC components from the desired DC output.

[2]AA centre frequency is 110MHz

6.3 UV Doppler Free Absorption Signal

To get the absorption signal, we do amplitude modulation of the AOM, i.e. the AOM is periodically switched on and off, which works in a same way as a chopper. Only the probe beam is periodically interrupted, not the noise. So the noise will be removed from the output of the Lock-in amplifier since the centre frequency of the filter is locked onto the modulation frequency and only the absorption signal will survived.

Fig(6.6) shows the UV Doppler free absorption signal. The modulation frequency of the AOM is $25KHz$. The pump beam is about $1mW$ and probe beam is about $100uW$.

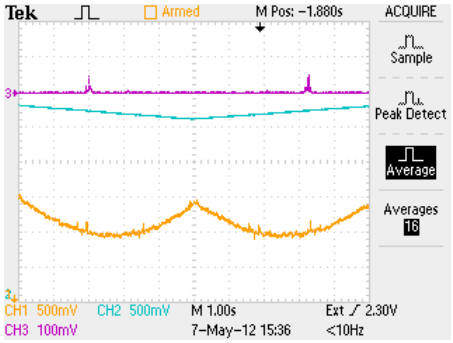

(a) Pump-probe configuration with pump beam on.

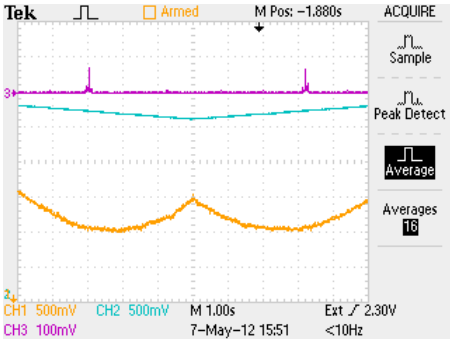

(b) Pump-probe configuration with pump beam blocked.

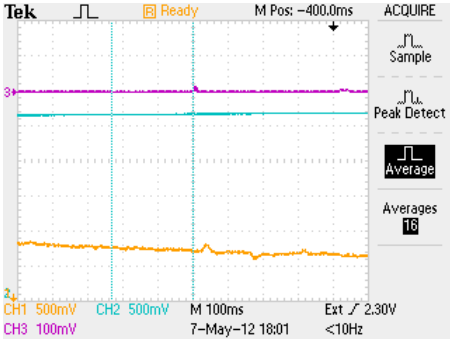

(c) A zoomed in look with pump beam on.

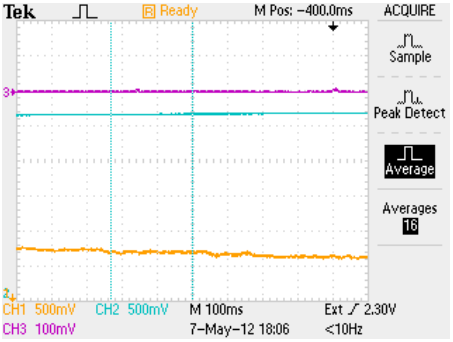

(d) A zoomed in look with pump beam blocked.

Figure 6.6: UV Doppler free absorption signal. With pump beam blocked, the yellow line shows the Doppler broadening signal. The hyperfine structure peaks appear when the pump beam is on. The fundamental light of the SHG laser is scanned from $646.72123nm$ to $646.72434nm$[3]. The heat pipe oven with $5.3 \times 10^{-3} mbar$ Argon was heated to 400℃.

6.4 The Error Signal

In order to get the error signal, the driving frequency($105MHz$) of the AOM is modulated($208KHz$). The modulation frequency can be considered as a perturbation compared to light frequency($10^{15}Hz$). The error signal comes from the Taylor expansion. To see this process mathematically, the modulated laser frequency is written as below:

$$\omega_L = \omega_0 + A_m sin\left(\omega_m t\right) \tag{6.1}$$

Assume that the modulation frequency much slower than laser frequency, $\omega_m << \omega_0$. A_m is the modulation amplitude. So that absorption signal $S\left(\omega_L\right)$ can be Taylor expanded,

$$\begin{aligned} S\left(\omega_L\right) &= S\left(\omega_0\right) + S'\left(\omega_0\right)\left(\omega_L - \omega_0\right) + O\left(\left(\omega_m\right)^2\right) && (6.2)\\ &= S\left(\omega_0\right) + S'\left(\omega_0\right) A_m sin\left(\omega_m t\right) && (6.3) \end{aligned}$$

higher order terms are ignored. The phase shifter in lock-in amplifier gives a phase shift ϕ to the reference signal, $A_r sin\left(\omega_m t + \phi\right)$. The mixer multiplies two signals together:

$$\begin{aligned} S\left(\omega_L\right) \times A_r sin\left(\omega_m t + \phi\right) &= \left[S\left(\omega_0\right) + S'\left(\omega_0\right) A_m sin\left(\omega_m t\right)\right] A_r sin\left(\omega_m t + \phi\right) \\ &= S\left(\omega_0\right) A_r sin\left(\omega_m t + \phi\right) \\ &+ S'\left(\omega_0\right) A_m A_r sin\left(\omega_m t\right) sin\left(\omega_m t + \phi\right) \\ &= S\left(\omega_0\right) A_r sin\left(\omega_m t + \phi\right) + \frac{1}{2} S'\left(\omega_0\right) A_m A_r cos\left(\phi\right) \\ &- \frac{1}{2} S'\left(\omega_0\right) A_m A_r cos\left(2\omega_m t + \phi\right) \end{aligned} \tag{6.4}$$

Passing through the low-pass filter, the oscillation terms are removed. Thus, we get the error signal:

$$E\left(\omega_L\right) \propto \frac{1}{2} S'\left(\omega_0\right) A_m A_r cos\left(\phi\right) \tag{6.5}$$

The error signal dependants on phase ϕ and proportional to A_m and A_r, Fig(6.7). UV laser can be locked in next step. UV MOT will be pursued soon.

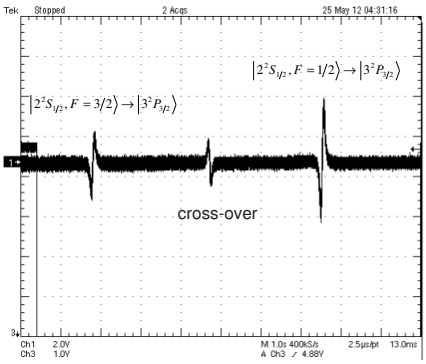

Figure 6.7: UV error signal. AOM modulation frequency is $208KHz$. Time constant of Lock-in amplifier is $100mS$.

7. Appendix

Fig(7.1).

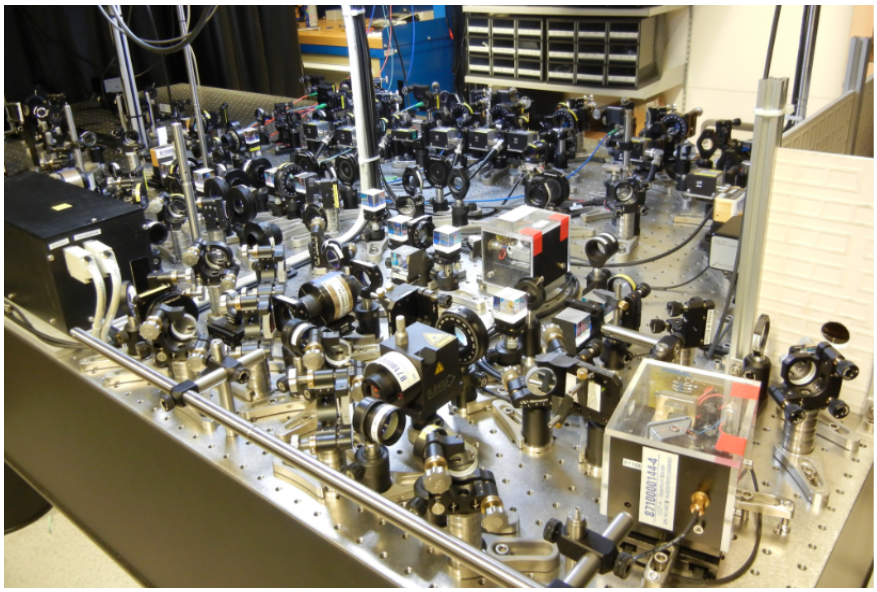

Figure 7.1: $671nm$ laser system table

Fig(7.2).

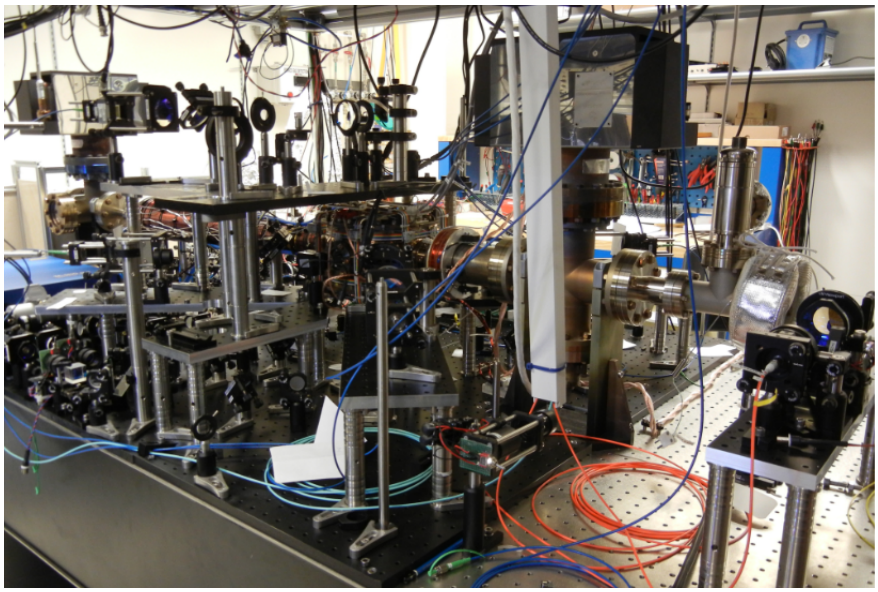

Figure 7.2: Vacuum system table

Fig(7.3).

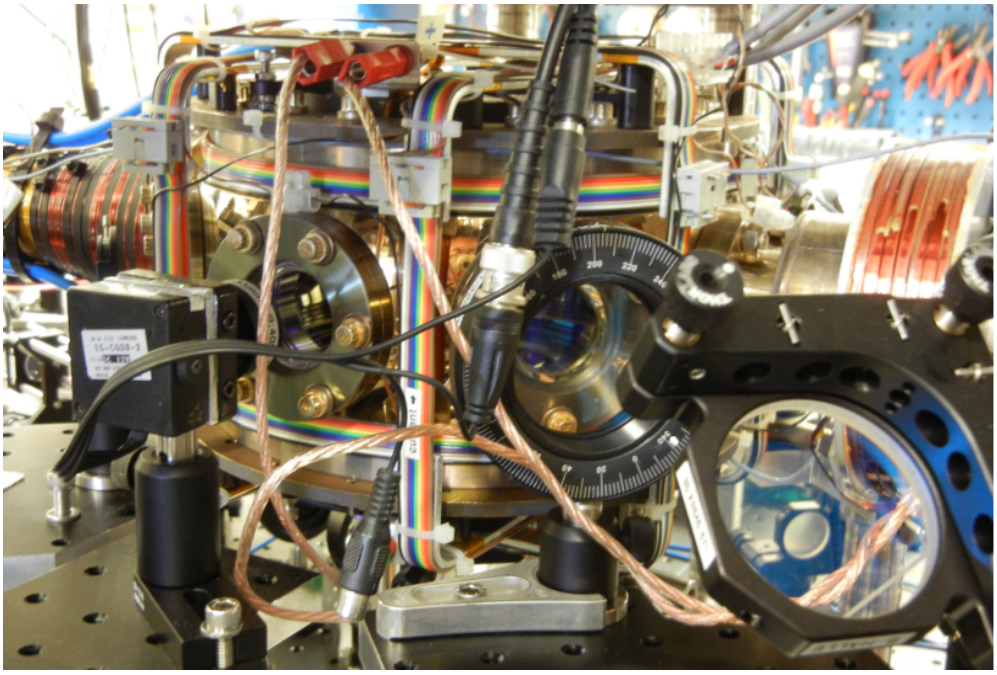

Figure 7.3: MOT chamber

Fig(7.4).

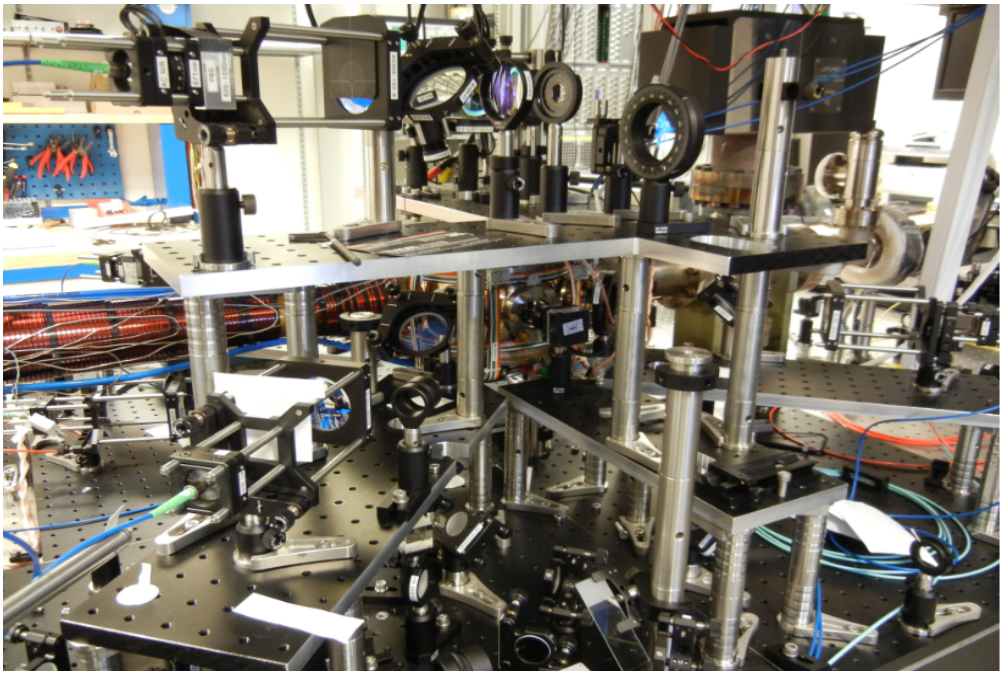

Figure 7.4: MOT optics

Fig(7.5).

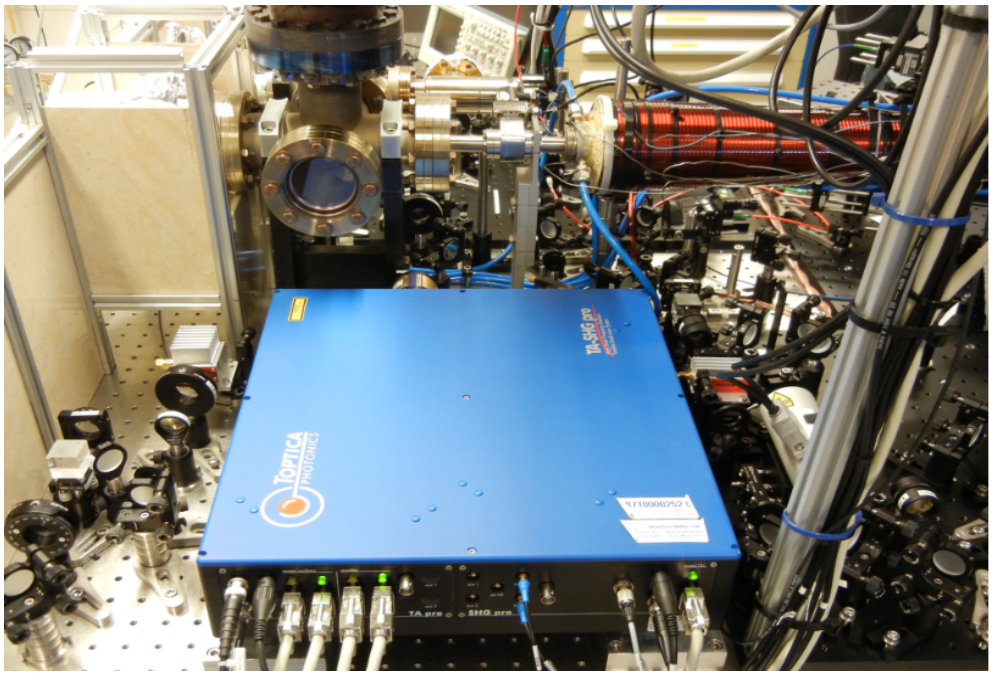

Figure 7.5: 323nm laser system

Fig(7.6).

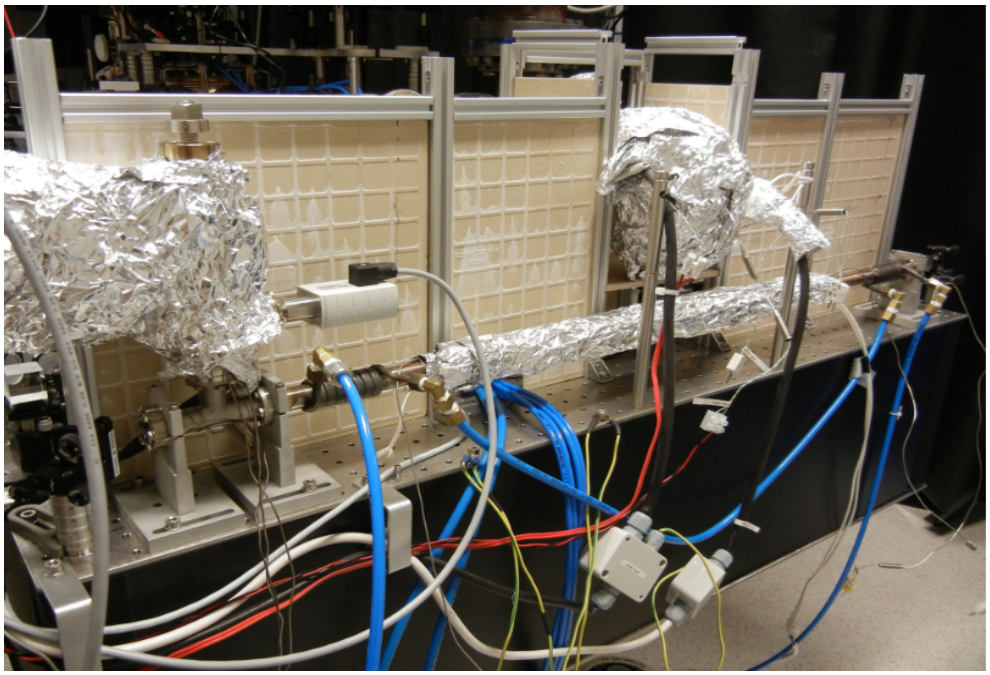

Figure 7.6: UV heat pipe oven

Bibliography

[1] M.R.Matthews C.E.Wieman E.A.Cornell M.H.Anderson, J.R.Ensher. Observation of bose-einstein condensation in a dilute atomic vapor. *Science*, 269:198, (1995).

[2] J.J.Tollett C.C.Bradley, C.A.Sackett and R.G.Hulet. Evidence of bose-einstein condensation in an atomic gas with attractive interactions. *Phys.Rev.Lett.*, 75:1687, (1995).

[3] M.R.Andrews N.J.van Druten D.S.Durfee D.M.Kurn K.B.Davis, M.O.Mewes and W.Ketterle. Bose-einstein condensation in a gas of sodium atoms. *Phys.Rev.Lett.*, 75:3969, (1995).

[4] S.N.Bose. *Z.Phys.*, 26:178, (1924).

[5] A.Einstein. *Sitzungsberichte der Preussischen Akademie der Wissenschaften*, 1:3, (1924).

[6] C.J.Joachain B.H.Bransden. *Physics of Atoms and Molecules*. Prentice Hall, second edition, 2003.

[7] B.DeMarco and D.S.Jin. Onset of fermi degeneracy in a trapped atomic gas. *Science*, 285:1703, (1999).

[8] P.Julienne C.Chin, R.Grimm and E.Tiesinga. Feshbach resonances in ultracold gases. *Rev. Mod. Phys.*, 82:1225, (2010).

[9] J.M.Gerton E.R.I.Abraham, W.I.McAlexander, R.G.Hulet R.Cote, and A.Dalgarno. Triplet s-wave resonance in ^6li collisions and scattering lengths of ^6li and ^7li. *Phys.Rev.A*, 55:R3299, (1997).

[10] R.Combescot. Trapped ^{6}li: A high tc superfluid? *Phys.Rev.Lett.*, 83:3766, (1999).

[11] K.M.O'Hara S.R.Granade, M.E.Gehm and J.E.Thomas. All-optical production of a degenerate fermi gas. *Phys.Rev.Lett.*, 88:120405, (2002).

[12] W.I.McAlexander G.B.Partridge R.G.Hulet A.G.Truscott, K.E.Strecker. Observation of fermi pressure in a gas of trapped atoms. *Science*, 291:2570, (2001).

[13] K.L.Corwin G.Ferrari T.Bourdel J.Cubizolles F.Schreck, L.Khaykovich and C.Salomon. Observation of fermi pressure in a gas of trapped atoms. *Phys.Rev.Lett.*, 87:080403, (2001).

[14] Immanuel Bloch. Ultracold quantum gases in optical lattices. *Nature Physics*, 1:23, (2005).

[15] F.D.M.Haldane. Model for a quantum hall effect without landau levels: Condensed-matter realization of the "parity anomaly". *Phys.Rev.Lett.*, 61:2015, (1988).

[16] Baigeng Wang Shi.Liang.Zhu and L.-M.Duan. Simulation and detection of dirac fermions with cold atoms in an optical lattice. *Phys.Rev.Lett.*, 98:260402, (2007).

[17] T.W.Hänsch and A.L.Schawlow. Cooling of gases by laser radiation. *Opt.Commun.*, 13:68, (1975).

[18] D.Wineland and H.Dehmelt. Proposed 10^{14} $dv < v$ laser fluorescence spectroscopy on tl+mono-ion oscillator iii (side band cooling). *Bull.Am.Phys.Soc.*, 20:637, (1975).

[19] W.D.Phillips and H.Metcalf. Laser deceleration of an atomic beam. *Phys.Rev.Lett.*, 48:596, (1982).

[20] M.D.Ray T.E.Barrett, S.W.Dapore-Schwartz and G.P.Lafyatis. Slowing atoms with σ^- polarized light. *Phys. Rev. Lett.*, 67:3483, (1991).

[21] J.E.Bjorkholm A.Cable S.Chu, L.Hollberf and A.Ashkin. Three-dimensional viscous confinement and cooling of atoms by resonance radiation pressure. *Phys.Rev.Lett.*, 55:48, (1985).

[22] C.I.Westbrook P.D.Lett, R.N.Watts and H.J.Metcalf W.D.Phillips, P.L.Gould. Observation of atoms laser cooled below the doppler limit. *Phys.Rev.Lett.*, 61:169, (1988).

[23] J.Dalibard and C.Cohen-Tannoudji. Laser cooling below the doppler limit by polarization gradients: simple theoretical models. *J.Opt.Soc.Am.B*, 6:2023, (1989).

[24] E.Riis P.J.Ungar, D.S.Weiss and Steven Chu. Optical molasses and multilevel atoms: theory. *J.Opt.Soc.Am.B*, 6:2058, (1989).

[25] Alex Cable Steven Chu E.L.Raab, M.Prentiss and D.E.Pritchard. Trapping of neutral sodium atoms with radiation pressure. *Phys. Rev. Lett.*, 59:2631, (1987).

[26] M.Zawada J.Zachorowski T.M.Brzozowski, M.Maczazyńska and W.Gawlik. Time-of-flight measurement of the temperature of cold atoms for short trapprobe beam distances. *J.Opt.B: Quantum Semiclass.Opt.*, 4:62, (2002).

[27] M.Taglieber. Quantum degeneracy in an atomic fermi-fermi-bose mixture. (2008).

[28] K.M.Birnbaum and The Quantum Optics Group. Ultra-high vacuum chambers. (2005).

[29] D.M.B.P.Milori J.Flemming, A.M.Tuboy. Magneto-optical trap for sodium atoms operating on the d1 line. *Opt.Commun.*, 135:269, (1997).

[30] M.Zielonkowski M.Weidemüller R.Grimm U.Schünemann, H.Engler. Magneto-optic trapping of lithium using semiconductor lasers. *Opt.Commun.*, 158:263, (1998).

[31] T.Esslinger A.Hemmerich C.Zimmermann V.Vuletic W.König T.W.Hänsch L.Ricci, M.Weidemüller. A compact grating-stabilized diode laser system for atomic physics. *Opt.Commun.*, 117:541, (1995).

[32] M.E.Gehm. Properties of ^6li. (2003).

[33] C.R.Vidal and J.Cooper. Heat-pipe oven: A new, well-defined metal vapor device for spectroscopic measurements. *J.Appl.Phys.*, 40(8):3370, (1969).

[34] C.R.Vidal and F.B.Haller. Heat pipe oven applications. i. isothermal heater of well defined temperature. ii. production of metal vapor-gas mixtures. *Rev.Sci.Instrum.*, 42(12):1779, (1971).

[35] P.M.Duarte. Narrow line laser cooling of lithium: A new tool for all-optical production of a degenerate fermi gas. (2011).

[36] A.L.Schawlow T.W.Hänsch and G.W.Series. The spectrum of atomic hydrogen. *Scientific American*, 240:72, (1979).

[37] J.Helmcke H.Stoehr, F.Mensing and U.Sterr. Diode laser with 1hz linewidth. *Optics Letters*, 31:736, (2006).

[38] G.C.Bjorklund and M.D.Levenson. Frequency modulation(fm) spectroscopy theory of lineshapes and signal-to-noise analysis. *Appl.Phys.B*, 32:145, (1983).

[39] F.Levi M.O.Tataw E.A.Donley, T.P.Heavner and S.R.Jefferts. Double-pass acousto-optic modulator system. *Rev.Sci.Instrum.*, 76:063112, (2005).

[40] R.J.C.Spreeuw D.Voigt, E.C.Schilder and H.B.van Linden van den Heuvell. Characterization of a high-power tapered semiconductor amplifier system. *Appl.Phys.B*, 72:279, (2001).

[41] J.M.Hitchcock T.A.Corcovilos T.-L.Yang A.Reed P.M.Duarte, R.A.Hart and R.G.Hulet. All-optical production of a lithium quantum gas using narrow-line laser cooling. *Phys. Rev. A*, 84:061406(R), (2011).

[42] W.L.Wiese and J.R.Fuhr. Accurate atomic transition probabilities for hydrogen, helium, and lithium. *J.Phys.Chem.Ref.Data*, 38:565, (2009).